Journal of Biomolecular NMR, **19:** 209–230, 2001.
KLUWER/ESCOM

Anisotropic rotational diffusion in model-free analysis for a ternary DHFR complex

Michael J. Osborne & Peter E. Wright*
Department of Molecular Biology and Skaggs Institute for Chemical Biology, The Scripps Research Institute, 10550 North Torrey Pines Road, La Jolla, CA 92037, U.S.A.

Received 4 August 2000; Accepted 5 December 2000

Key words: nuclear spin relaxation, protein dynamics, rotational diffusion anisotropy

Abstract

Model-free analysis has been extensively used to extract information on motions in proteins over a wide range of timescales from NMR relaxation data. We present a detailed analysis of the effects of rotational anisotropy on the model-free analysis of a ternary complex for dihydrofolate reductase (DHFR). Our findings show that the small degree of anisotropy exhibited by DHFR ($D_{||}/D_{\perp} = 1.18$) introduces erroneous motional models, mostly exchange terms, to over 50% of the NH spins analyzed when isotropic tumbling is assumed. Moreover, there is a systematic change in S^2, as large as 0.08 for some residues. The significant effects of anisotropic rotational diffusion on model-free motional parameters are in marked contrast to previous studies and are accentuated by lowering of the effective correlation time using isotropic tumbling methods. This is caused by the preponderance of NH vectors aligned perpendicular to the principal diffusion tensor axis and is readily detected because of the high quality of the relaxation data. A novel procedure, COPED (COmparison of Predicted and Experimental Diffusion tensors) is presented for distinguishing genuine motions from the effects of anisotropy by comparing experimental relaxation data and data predicted from hydrodynamic analyses. The procedure shows excellent agreement with the slow motions detected from the axially symmetric model-free analysis and represents an independent procedure for determining rotational diffusion and slow motions that can confirm or refute established procedures that rely on relaxation data. Our findings show that neglect of even small degrees of rotational diffusion anisotropy can introduce significant errors in model-free analysis when the data is of high quality. These errors can hinder our understanding of the role of internal motions in protein function.

Abbreviations: DHFR, *Escherichia coli* dihydrofolate reductase; T_1, longitudinal relaxation time constant; T_2, transverse relaxation time constant; CPMG, Carr–Purcell–Meiboom–Gill; NOE, nuclear Overhauser effect; 2D, 3D, two-, three-dimensional; DHNADPH, 5,6-dihydronicotinamide adenine dinucleotide phosphate, reduced; EDTA, ethylenediaminetetraacetic acid; DTT, dithiothreitol; ns, nanosecond; ps, picosecond; μs, microsecond; ms, millisecond; PDB, Protein Data Bank.

Introduction

Many treatises have recently appeared championing a functional role for motions in proteins (Cannon et al., 1996; Young and Post, 1996; Frauenfelder and McMahon, 1998; Zhou et al., 1998) based primarily on data from a variety of biophysical techniques such as NMR and elastic incoherent neutron scattering. However, conclusive evidence of a functional role for motions remains speculative, due in part to the mechanistic interpretation of the experimental results and the accuracy of the motional models chosen to describe internal dynamics.

The model-free formalism of Lipari and Szabo (1982a, b) has been extensively used to extract detailed dynamical information from NMR spin relax-

*To whom correspondence should be addressed. E-mail: wright@scripps.edu

ation data (T_1, T_2 and $\{^1H\}$-X NOE). This formalism describes internal dynamics in terms of an overall rotational diffusion tensor for the molecule, and a generalized order parameter (S^2) and internal correlation time (τ_e) for each nuclear spin. The order parameter provides a direct physical interpretation of dynamics, and for this reason, the model-free analysis has been preferred over other methods, such as direct mapping of the spectral density function (Peng and Wagner, 1992; Farrow et al., 1995), to analyze NMR relaxation data.

The integrity of the results from model-free analyses, specifically the assignment of motions on timescales that are potentially important for protein function, has recently been questioned. For well-structured proteins, nuclear relaxation is dominated by the overall tumbling which can be described by the rotational diffusion tensor. Accurate determination of the diffusion tensor is crucial for separating the effects of overall motion from internal motions and hence extracting reliable model-free parameters. Thus, Korzhnev et al. (1997) have demonstrated that an incorrect overall correlation time (τ_c) can be derived from the T_1/T_2 ratios when motions in a protein are extensive and are dominated by fluctuations on the nanosecond timescale: these motions can go undetected in the subsequent model-free analysis. The assumption of isotropic rotational diffusion in model-free analyses is commonly made to simplify the model-free spectral density function. It has recently been shown, however, that neglect of anisotropic tumbling in the model-free analysis can result in the introduction of erroneous motional models on both the ns and ms–μs timescales, depending on the orientation of the NH vector with respect to the principal axis of the rotational diffusion tensor (Barbato et al., 1992; Schurr et al., 1994; Tjandra et al., 1995a, b, 1996; Mandel et al., 1996; Luginbühl et al., 1997; Gagné et al., 1998). It is still unclear, however, to what extent inaccuracies in the description of overall rotational diffusion can affect the model-free analysis and how genuine motions can be distinguished from artifacts resulting from use of an incorrect diffusion model.

Previous model-free analyses assuming isotropic diffusion for systems that tumble anisotropically suggest that the effects of neglecting the anisotropy are only moderate, leading to a small number of erroneous motions on the ns or ms–μs timescales. Moreover, the value of S^2 seems to be largely unaffected (Barbato et al., 1992; Schurr et al., 1994; Tjandra et al., 1995a, b, 1996; Mandel et al., 1996; Luginbühl et al., 1997; Gagné et al., 1998).

In this paper, model-free analyses assuming isotropic and axially symmetric diffusion tensors are presented for relaxation data on a ternary complex of dihydrofolate reductase (DHFR) with folate and 5,6-dihydroNADPH (DHNADPH). Assumption of isotropic tumbling in this weakly anisotropic system ($D_{||}/D_{\perp} = 1.18$) results in the attribution of erroneous motions, mostly exchange contributions, to $\sim$50% of the residues. There is also a significant change in the S^2 for residues requiring erroneous exchange terms. Thus, accurate characterization of the diffusion tensor is a necessary prerequisite for obtaining reliable results from the model-free analysis. Methods for determining the degree of rotational diffusion anisotropy from relaxation data (Brüschweiler et al., 1995; Tjandra et al., 1995b; Zheng et al., 1995; Lee et al., 1997) depend on recognition and exclusion of residues displaying significant internal motion from the analysis. This is usually achieved using T_1/T_2 ratios, but is difficult in non-isotropic systems (Kroenke et al., 1998). In this paper, we introduce a novel procedure for identifying genuine motions in the presence of anisotropic tumbling. This procedure, termed COPED (COmparison of Predicted and Experimental Diffusion tensors), identifies motions by comparing diffusion coefficients determined from relaxation data and from hydrodynamic analyses. Motions identified from the COPED analysis are in excellent agreement with motions determined from the axially symmetric model-free analysis for the ternary DHFR complex.

Theory

Axially symmetric model-free spectral density function

The model-free method (Lipari and Szabo, 1982a, b) has been used extensively to extract information on motional amplitudes and timescales. For proteins that display axial symmetry, the D_{xx} and D_{yy} components of the diffusion tensor are equal, and overall rotational diffusion can be described by three parameters; θ, the angle the NH vector makes with the principal axis of the diffusion tensor, and $D_{||}$ and $D_{\perp}$, the diffusion coefficients parallel and perpendicular to the principal axis of the diffusion tensor, respectively (Woessner, 1962). These terms are related to the model-free spectral density function for axially symmetric overall rotational tumbling, e.g. (Halle and Wennerström, 1981;

Lipari and Szabo, 1982a,b; Schurr et al., 1994; Zheng et al., 1995):

$$J(\omega) = \frac{2}{5}\left\{S^2\left[\sum_{k=1..3}^{3}\frac{A_k\tau_k}{1+\omega^2\tau_k^2}\right] + \left(1-S^2\right)\left[\sum_{k=1..3}^{3}\frac{A_k\tau_k^{'}}{1+\left(\omega\tau_k^{'}\right)^2}\right]\right\} \quad (1)$$

in which $A_1 = (3/4)\sin^4\theta$, $A_2 = 3\sin^2\theta\cos^2\theta$, $A_3 = (3\cos^2\theta - 1)^2/4$, and the correlation times τ_1, τ_2 and τ_3 depend on the rotational diffusion coefficients by the relations: $\tau_1 = (4D_{||} + 2D_{\perp})^{-1}$; $\tau_2 = (D_{||} + 5D_{\perp})^{-1}$, $\tau_3 = (6D_{\perp})^{-1}$. The generalized order parameter (S^2) describes the amplitude of the internal motion and can range from 0 for unrestricted motion to 1 for a fixed vector. $\tau_k^{'}$ is the effective correlation time and is dependent on τ_e, the internal correlation time for fast internal motions ($\tau_e \ll \tau_k$): $\tau_k^{'} = \tau_k\tau_e/(\tau_k + \tau_e)$. If τ_e is fast and the internal motion is in the extreme narrowing limit, $\omega\tau_c \ll 1$, Equation 1 becomes:

$$J(\omega) = \frac{2}{5}\left\{S^2\left[\sum_{k=1..3}^{3}\frac{A_k\tau_k}{1+\omega^2\tau_k^2}\right]\right\} \quad (2)$$

For isotropic tumbling, the three components of the diffusion tensor are equal ($D_{iso} = D_{zz} = D_{yy} = D_{xx}$) and the effective rotational correlation time is constant, described by a single correlation time ($\tau_c = 1/6D_{iso}$). Since rotation of a sphere will be random, there is no dependence on θ, the value of A is meaningless and the equation reduces to the well-known isotropic model-free spectral density (Lipari and Szabo, 1982a,b).

Detection of anisotropic tumbling

The degree of anisotropy can be determined experimentally from the local diffusion coefficients (D_i=1/6τ_{ci}) (Brüschweiler et al., 1995; Lee et al., 1997) or R_2/R_1 ratios (Tjandra et al., 1995b; Zheng et al., 1995). Expressions for transforming the structural coordinates from the molecular reference frame to the diffusion reference frame for isotropic, axially symmetric and anisotropic diffusion models based on local diffusion coefficients have been described by Brüschweiler et al. (1995) and Lee et al. (1997). For the axially symmetric diffusion tensor, values of $D_{\perp}$, $D_{||}$ and θ are determined by non-linear least squares optimization, and are used to describe the diffusion tensor in the axially symmetric model-free analysis (Equation 1). The accuracy of the diffusion tensor relies on excluding spins undergoing slow motions ($\tau_e \gg 100$ ps. Note that in this paper slow motions refer to both ns and ms–μs motions) from the analysis and on the distribution of NH bond vector orientations in the diffusion frame (Lee et al., 1997; Kroenke et al., 1998). Identification of residues exhibiting slow motions can be difficult using methods based primarily on T_1/T_2 ratios, particularly when the protein is dominated by slow motions (Korzhnev et al., 1997) or displays anisotropic rotational diffusion (Kroenke et al., 1998).

Detecting motions in the presence of anisotropy – COPED

Hydrodynamic analyses based on atomic coordinates represent an alternative procedure for estimating the diffusion tensor (Woessner, 1962; Garcia de la Torre, 1981). In this procedure, all motions are assumed to be fast. Thus, differences in the local diffusion coefficients determined experimentally from relaxation data and predicted from hydrodynamic calculations can potentially distinguish genuine motions from the effects of anisotropy. In the principal axis frame of the axially symmetric diffusion tensor, differences can be easily evaluated from the linear relationship (Lee et al., 1997):

$$D = D_{iso} - \left(3\cos^2\theta - 1\right)\left(D_{||} - D_{\perp}\right)/6 \quad (3)$$

in which D_{iso}= $(2D_{\perp} + D_{||})$ /3. Using Equation 3, we show that genuine motions in the ternary DHFR complex can be distinguished from the effects of anisotropy by comparison of the local diffusion coefficients calculated from relaxation data and from hydrodynamic analyses, a procedure we term COPED. Application of COPED to the ternary DHFR complex studied here shows that COPED is superior to the isotropic model-free analysis for identifying motions in the presence of anisotropic tumbling. The results from COPED are in excellent agreement with a model-free analysis assuming axially symmetric rotational diffusion.

Materials and methods

Sample preparation

^{15}N-labeled DHFR was expressed in *E. coli* BL21 (DE3) cells using a pET-22b-derived plasmid (kindly provided by S.J. Benkovic) in minimal medium containing $(^{15}NH_4)_2SO_4$ (2 g/l). Expression and purification were performed as described previously (Miller

and Benkovic, 1998). The NMR sample was prepared by exchange into argon-saturated NMR buffer (0.1 M KCl, 1 mM EDTA, 1 mM [^{2}H]DTT, 50 mM potassium phosphate, pH 6.8) by elution from NAP-5 or NAP-25 columns and concentrated to a volume of $\sim$300 μL. DHFR concentration was determined spectrophotometrically using a molar extinction coefficient of 31 100 M^{-1} cm^{-1} (Epstein et al., 1995). Stock 0.1 M samples of folate (Sigma) and DHNADPH (kindly provided by S.J. Benkovic and G.P. Miller) were prepared in NMR buffer, and added to the DHFR sample so that both cofactor and substrate were in approximately sixfold excess. The final concentration of DHFR in the NMR sample was $\sim$1.7 mM.

NMR spectroscopy and data processing

The ^{15}N relaxation parameters, T_1, T_2, and steady-state {^{1}H}-^{15}N NOEs, were acquired using pulse sequences described by Farrow et al. (1995) on Bruker DRX and AMX II spectrometers operating at ^{1}H Larmor frequencies of 600.13 and 500.37 MHz, respectively. Spectra were recorded at 306.4 K (calibrated with neat methanol (Orbons et al., 1987)). ^{15}N T_2 and NOE data were acquired at both frequencies. ^{15}N T_1 data were acquired at 600 MHz only. Ten different T_1 relaxation delay time points were collected at 10, 50, 100, 200, 400, 700, 1000, 1500, 2000 and 3000 ms. Duplicate data sets were acquired for delays of 10, 400, and 1500 ms. The T_2 data were acquired at 6, 22, 42, 70, 122, 162, 202, 282 and 362 ms, with duplicate measurements at 6, 70 and 202 ms. The delay between ^{15}N 180° pulses in the CPMG sequence was 1 ms. The {^{1}H}-^{15}N steady state heteronuclear NOE was acquired in an interleaved manner in which each individual FID was collected with and without proton presaturation. The {^{1}H}-^{15}N NOE experiment was repeated four times. Recovery delays of 2.5 s, 2.5 s and 4.0 s were employed for the T_1, T_2, and NOE measurements, respectively.

Data were processed using Felix95 (Molecular Simulations, Inc.). Time domain data were zero-filled once and apodized with exponential, cosine-squared or Lorentzian-to-Gaussian window functions, depending on the degree of resonance overlap. T_1, T_2 and NOE values were determined from peak heights as described by Stone et al. (1992, 1993) using in-house macros and/or programs provided by A.G. Palmer. Uncertainties in NOEs were calculated as described by Nicholson et al. (1992).

Isotropic model-free analysis

Model-free analysis assuming isotropic rotational diffusion was performed using the method described by Mandel et al. (1995). Five motional models were used to fit the relaxation data after initial estimation of τ_c from the average T_1/T_2 ratio. These are: Model 1 (S^2); Model 2 (S^2 and τ_e); Model 3 (S^2 and R_{ex}); Model 4 (S^2, τ_e and R_{ex}); Model 5, the extended model proposed by Clore et al. (1990a). Relaxation data were fit to the dynamic models using the program ModelFree (version 3.1; Palmer et al., 1991) by minimizing the χ^2 error function, as previously described by Mandel et al. (1995). Five hundred Monte Carlo simulations were used to obtain statistical uncertainties. The goodness of fit between the experimental data and motional model was assessed by comparing the minimal value of the χ^2 function at the 95% confidence level (the $\alpha = 0.05$ critical value) of the χ^2 distribution determined from Monte Carlo simulations. F-statistical testing as described by Mandel et al. (1995) was used to select the appropriate motional model for each spin. The more complicated model was rejected where the reduction of χ^2 was less than the $\alpha = 0.10$ critical value for random statistical improvement. The internal parameters for the selected models of each NH vector were then simultaneously optimized with the global correlation time. If necessary, the selection procedure was cycled to obtain a convergent, self-consistent description of the data. We note that other workers (Phan et al., 1996) have excluded Model 5 from model selection since this model can introduce erroneous motions to compensate for anisotropic tumbling. Thus, in addition to F-testing, spins were assigned to Model 5 when the next best fit model (normally Model 2) exhibited a large value for χ^2 (normally in excess of 40).

Structure coordinates

A 3D structure for the ternary DHFR:folate:DHNADPH complex has not been reported. A recent survey by Sawaya and Kraut (1997) on over 45 X-ray structures of *E. coli* DHFR complexes showed that the 3D structures are highly conserved except in regions involving loop 1 (residues 9–24), and the βF-βG loop (residues 117–131). The loop 1 region adopts three distinct conformations, termed open, closed and occluded in various crystalline forms. These three conformations are characterized by the coordinate sets designated 1ra2, 1rx2, and 1rx7, respectively in the Brookhaven Protein Data Bank and these were used as inputs for hydrodynamic and inertia tensor calculations. Hydrogen atoms were added using InsightII

(Molecular Simulations, Inc.) and the resulting structures were subjected to 50 cycles of Powell minimization to alleviate poor non-bonded contacts.

Hydrodynamic calculations and inertia calculations

Hydrodynamic modeling and inertial tensor calculations were performed on the X-ray coordinates using an in-house program, MASH (written by Ishwar Radhakrishnan), which incorporates the HYDRO suite of programs of Garcia de la Torre (1981). Each residue was modeled as a single bead centered on the C^{α} atom. The viscosity was that of water at 306.4 K. The C^{α} bead radius was altered until the error function, $\Gamma = \Sigma\eta_i^2$, was minimized, where η_i^2 compares the goodness of fit of the calculated local diffusion coefficients ($D_{i(pred)}$) with the experimentally determined local diffusion coefficient ($D_{i(exp)}$). Values and errors for $D_{i(exp)}$ were obtained from T_1/T_2 ratios at 600 MHz using the 'tmest' program (Palmer, 2000). If desired the COPED procedure can be repeated after removal of residues exhibiting slow motions; however, this is generally unnecessary since the diffusion tensor from hydrodynamic modelling is largely independent of the relaxation data (see Results below). Coordinates of the structure are output within the frame of reference of the diffusion tensor. Other output from the program includes the local θ and ϕ angles for NH or other bond vectors (with respect to the diffusion tensor frame), the local correlation time (τ_{ci}) and the principal components of the global rotational diffusion tensor.

Identifying genuine motions using COPED for estimation of the diffusion tensor

The calculated diffusion tensor from the program MASH was used to predict the effects of axially anisotropic tumbling on local diffusion coefficients ($D_{i(pred)}$) by solving the linear relationship given in Equation 3. The experimental local diffusion coefficient ($D_{i(exp)}$) for each NH spin was plotted versus the value of θ determined from the MASH analysis to graphically identify residues undergoing motions. The goodness of fit between diffusion coefficients, calculated from the relaxation data and the predicted diffusion tensor, was estimated by a χ^2 statistic (N.B.: to prevent confusion with the χ^2 error function used in the program ModelFree, the symbol η^2 is used here) defined as: $\eta_i^2 = (D_{i(exp)} - D_{i(pred)}/\sigma)^2$, where σ is the uncertainty in $D_{i(exp)}$. Residues exhibiting small values of η_i^2 were identified as having fast motions (see Results for further details) and included for the subsequent fitting of the diffusion tensor described in the next section. Spins undergoing ms–μs or ns–ps timescale motions were identified from negative or positive values, respectively, of $D_{i(exp)} - D_{i(pred)}$, in addition to exhibiting large values of η_i^2.

Calculation of the diffusion tensor from T_1/T_2 ratios

The principal components (D_{zz}, D_{xx}, D_{yy}), $D_{\perp}$ and $D_{||}$, and the orientation of the diffusion tensor relative to the molecular frame were calculated using the program quadric_diffusion kindly provided by Dr. Arthur Palmer (Lee et al., 1997; Palmer, 2000). In the absence of a structure for the specific ternary complex studied herein, we fitted $D_{i(exp)}$ to the three coordinate sets 1rx2, 1rx7 and 1ra2. Residues undergoing significant internal motions on the ps–ns timescales and ms–μs timescales were identified by COPED and excluded from the calculations. F-statistical testing was used to evaluate the significance of the isotropic, axially symmetric and anisotropic tensor models in the analysis.

Axially anisotropic model-free analysis

The program ModelFree (version 4.01; Palmer, 2000) was used to optimize Equation 1 based on the following relaxation data sets: $T_{1(600)}$, $T_{2(600)}$, $T_{2(500)}$, $NOE_{(600)}$ and $NOE_{(500)}$. Initial, fixed, values of the diffusion tensor (θ, $D_{\perp}$ and $D_{||}$) were obtained from the rotational diffusion analyses. Based on these values, models were selected for Models 1 to 4 in an analogous manner to the isotropic model-free approach. We note that no theoretical derivations have been reported for axially symmetric overall diffusion and a spectral density function for Model 5. Thus, spins requiring the two-timescale model were confirmed using other means (e.g. failing the linear relationship in Equation 3).

Based on the selected motional models, the overall rotational diffusion tensor (D_{iso}, $D_{||}/D_{\perp}$, and θ) was optimized simultaneously with the internal motional parameters for each spin. We optimized the diffusion tensor based on spins fit with Models 1 to 4 and a subset of these spins which satisfied the data according to the $\alpha = 0.05$ critical level.

Relaxation data simulations

Relaxation data (R_1, R_2 and NOE) were simulated using in-house programs. Simulations assumed either an isotropic or an axially symmetric diffusion tensor. In general, random values of θ, and/or internal motional

parameters within a specified range were used. Specific details for the simulated data sets are given in the Results section.

Reduced spectral density mapping

The reduced spectral density provides values of $J(0)$, $J(\omega_N)$ and $J(0.87\omega_H)$ from the relaxation data by assuming that the variation in $J(\omega)$ is smooth between $J(\omega_H + \omega_N)$ and $J(\omega_H - \omega_N)$. In the present case, we solved the modified spectral density equations using the method proposed by Farrow et al. (1995). Values of S^2 were estimated from the reduced spectral densities as described previously (Lefèvre et al., 1996; Bracken et al., 1999).

Results and discussion

R_1, R_2, and NOE data

The assignments for the ternary DHFR:folate: DHNADPH complex will be described elsewhere (M.J. Osborne and P.E. Wright, in preparation). At 600 MHz, 115 of the backbone ^{1}H-^{15}N cross peaks were sufficiently well resolved to allow accurate intensity measurements; at 500 MHz, this number was 85.

The relaxation data are shown in Figure 1 as a function of residue number. Standard errors obtained from multiple data sets show the data to be of high quality: the average errors are 1.2% for the $R_{1(600)}$ data set; 1.7% and 1.6% for the $R_{2(600)}$ and $R_{2(500)}$ data sets, respectively, and 3.5% and 4.5% for the $NOE_{(600)}$and $NOE_{(500)}$ data sets, respectively. These errors are small and are unlikely to bias the selection procedure in the model-free analysis towards the simpler model when internal motions are present (Mandel et al., 1995).

Hydrodynamic and inertia tensor calculations

The diffusion parameters calculated by hydrodynamics for the three representative sets of coordinates of DHFR complexes are shown in Table 1. A C^α bead radius of 3.19 Å was required to minimise Γ for each coordinate data set. The inertia and diffusion tensors are almost collinear (data not shown). The predicted anisotropy for DHFR is small and, based on previous studies, is not expected to greatly influence the model-free analysis under the assumption of an isotropic diffusion tensor (Barbato et al., 1992; Schurr et al., 1994; Tjandra et al., 1995a, b, 1996; Mandel et al., 1996; Luginbühl et al., 1997; Gagné et al., 1998).

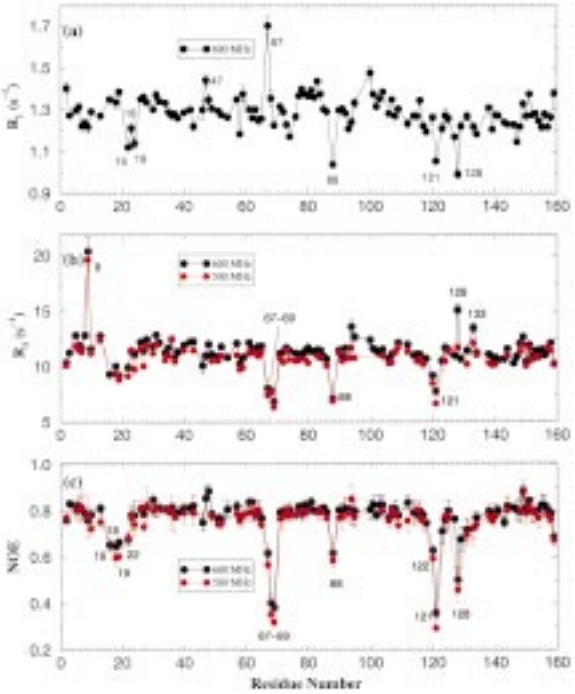

Figure 1. Plots of (a) R_1, (b) R_2, and (c) the $\{^1H\}$-^{15}N heteronuclear NOE as a function of residue number for the ternary DHFR–folate–DHNADPH complex. Data acquired at ^{1}H frequencies of 600 MHz and 500 MHz are shown as black and red circles, respectively.

The effects of anisotropic rotational diffusion on the model-free analysis, however, are highly dependent on the distribution of θ for the NH vectors (Lee et al., 1997). The maximum change in τ_{ci} predicted for the anisotropies described in Table 1 is $\sim$0.77 ns. This is much larger than the average error associated with τ_{ci} ($\sim$0.13 ns), indicating that the relaxation data will be influenced by the anisotropy (Tjandra et al., 1996; Lee et al., 1997). Given the relative spatial arrangement of the secondary structure elements in DHFR, an even distribution of NH vectors with respect to the diffusion tensor is expected. The present data, therefore, provide an excellent opportunity to study the effects of slight rotational diffusion anisotropy on isotropic model-free analysis and compare the results to the model-free analysis assuming an axially symmetric diffusion tensor model. Moreover, the data will test the usefulness of the COPED procedure for identifying slow motions in the presence of anisotropy.

Table 1. Calculated diffusion parameters from hydrodynamic analyses[a]

PDB	τ_c[b] (ns)	$2D_{zz}/(D_{xx}+D_{yy})$	D_{xx}/D_{yy}	R_{ex}[c]	ns–ps[d]
1rx2	9.02	1.16	1.06	5, **8**, **9**, 52, 94, 112, **127**, **128**, **133**	**2**, **16**, **18**, **19**, 34, 47, 57, 59, 64, **67**, **68**, **69**, 77, 78, 79, 81, 83, 86, **88**, 107, **120**, **121**, 140, **143**, 150, **159**
1rx7	9.05	1.16	1.06	5, **8**, **9**, 94, 112, **127**, **128**, **133**	**2**, **16**, **18**, **19**, 34, 47, 59, 62, **67**, **68**, **69**, **77**, 78, 79, 81, 83, **86**, **88**, 107,**120**, **121**, 140, **143**, 150, **159**
1ra2	9.07	1.16	1.06	5, **8**, **9**, 94, 112,**127**, **128**, **133**	**2**, **16**, **18**, **19**, 34, 47, 59, 62, **67**, **68**, **69**, **77**, 78, 79, 81, 83, **86**, **88**, 107, **120**, **121**, 140, **143**, 150, **159**

[a]To minimize Γ a value of 3.19 Å was required for the C^{α} bead radius for all sets of coordinates.
[b]$\tau_c = (6D_{iso})^{-1}$, $D_{iso} = (D_{zz} + D_{xx} + D_{yy})/3$.
[c]Determined from residues with a negative value for $D_{i(exp)} - D_{i(pred)}$ and satisfying $\eta_i^2 > 6$ (all residues) and $\eta_i^2 > 15$ (bold).
[d]Determined from residues with a positive value for $D_{i(exp)} - D_{i(pred)}$ and satisfying $\eta_i^2 > 6$ (all residues) and $\eta_i^2 > 15$ (bold).

Model-free analysis assuming isotropic tumbling

Estimation of τ_c

The global, isotropic correlation time τ_c was estimated from the T_1/T_2 ratios of residues exhibiting fast motions. Exchange contributions for residues 8, 9, 94, 128 and 133 were identified using the procedure of Tjandra et al. (1996). Residues undergoing motions slower than 100 ps and faster than τ_c were identified from low NOE values (< 0.65 at 600 MHz) (Kay et al., 1989b). τ_c was then estimated to be 8.98 ± 0.05 ns from the mean T_1/T_2 ratio of the remaining residues; the 10% trimmed weighted mean T_1/T_2 ratio yielded a very similar value of 9.01 ± 0.05 ns.

Model selection

Isotropic model-free analyses were performed at two fields for the 85 residues that could be resolved at both 500 and 600 MHz. A single field analysis for the 115 residues resolved at 600 MHz was also performed. The model-free parameters reported are for the data calculated at two fields unless the amide resonance was not resolved at 500 MHz; in this case, the single field (600 MHz) values are reported. R_{ex} terms are quoted for 600 MHz.

To obtain a convergent, self-consistent description of the data it was necessary to cycle the model-selection process three times. Table 2 summarizes the selected models at different cycles of the analysis for both two-field and single-field (600 MHz) analyses. Figure 2 shows values for S^2 and R_{ex} calculated after optimization at the initial τ_c (8.98 ns) and the final τ_c (8.70 ns).

The number of residues requiring ns motions (Model 5) is independent of the value of τ_c (Table 2). This is due, in part, to the stringent criteria used in assigning spins to Model 5 (for other reasons, see below). The most striking feature of the analyses is the influence of the rotational correlation time, τ_c, on the selection of motional models and hence on the assignment of internal motions to individual spins.

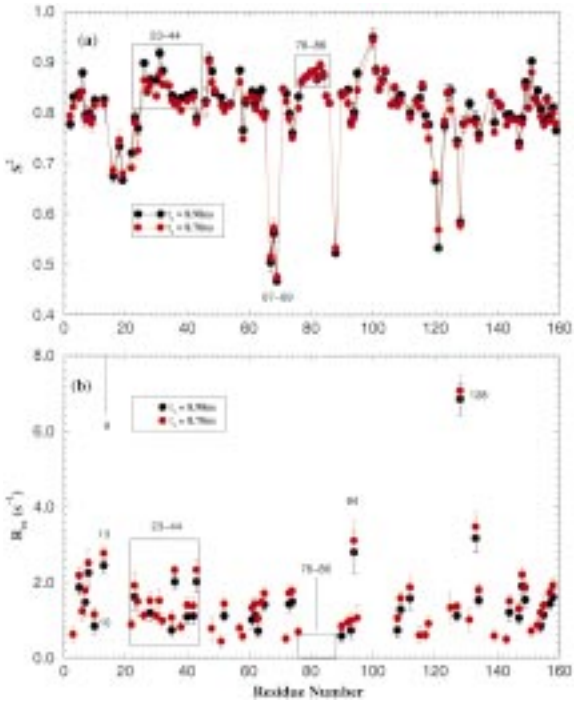

Figure 2. Plots of the isotropic model-free internal motional parameters S^2 (a) and R_{ex} (b) as a function of residue number for the ternary DHFR–folate–DHNADPH complex. Black circles correspond to values obtained using model selection for an initial rotational correlation time (τ_c) of 8.98 ns obtained from the T_1/T_2 ratio (see text). Red circles describe internal motional parameters selected for a rotational correlation time (τ_c) of 8.70 ns, which was the final optimized value, obtained after the third cycle of the model selection procedure (see text). For clarity R_{ex} values <8 s^{-1} are displayed (b). Residue 9 has an R_{ex} value greater than 10 s^{-1} for both analyses and is not represented in panel b.

Table 2. Model selection for isotropic model-free analysis

	Two field						Single field					
Cycle	τ_c (ns)	S^2	S^2,τ_e	S^2,R_{ex}	S^2,τ_e,R_{ex}	S_s^2,S_f^2	τ_c (ns)	S^2	S^2,τ_e	S^2,R_{ex}	S^2,τ_e,R_{ex}	S_s^2,S_f^2
Initial	8.98	23	19	23	10	10	8.98	40	32	24	8	11
2	8.83	13	15	36	11	10	8.82	34	16	44	10	11
3	8.70	13	9	38	15	10	8.69	29	12	49	14	11
Diff	−0.28	−10	−10	+15	+5	0	−0.29	−11	−20	+25	+6	0

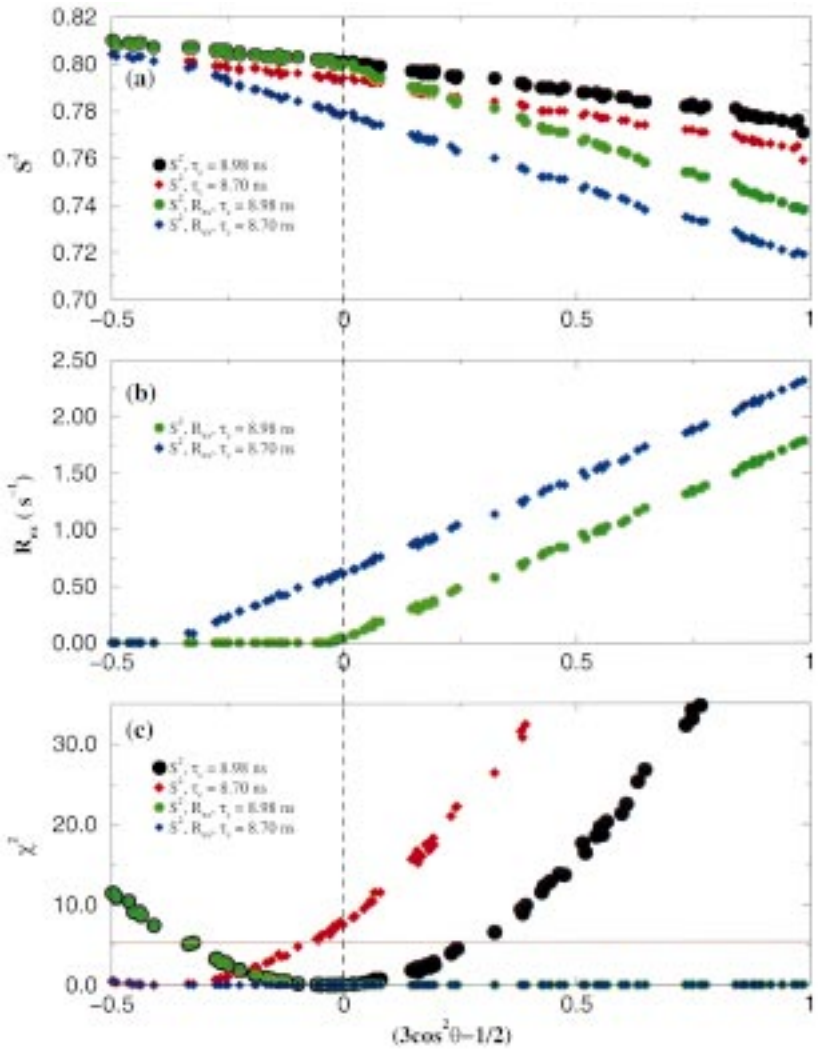

Figure 3. The effects of the rotational correlation time τ_c and axially symmetric rotational diffusion anisotropy on S^2 (a), R_{ex} (b) and the error function, χ^2 (at the $\alpha = 0.05$ critical value) (c) on the isotropic model-free analysis. Relaxation data (R_1, R_2 and NOE) were simulated for 100 spins with internal motional parameters of $S^2 = 0.8$, $R_{ex} = \tau_e = 0$. θ was randomly assigned a value between 0 and 90°; the degree of axially symmetric anisotropy, $D_{||}/D_{\perp}$ was set to 1.3 and $1/6D_{iso} = 8.98$ ns. Errors for R_1, R_2 and NOE were 1.2%, 1.7% and 3.5%, respectively. The vertical dashed line represents the isotropic case (i.e. $\theta = 54.7°$). Solid circles represent model-free parameters obtained by fitting the simulated relaxation data to Model 1 (optimizing S^2 only) for correlation times of 8.98 ns (black circles) and 8.70 ns (red diamonds). Model-free parameters obtained using Model 3 (S^2 and R_{ex}) are represented by green circles ($\tau_c = 8.98$ ns) and blue diamonds ($\tau_c = 8.70$ ns). The simulated data were fitted assuming isotropic tumbling.

A decrease in τ_c markedly increases the number of spins requiring exchange contributions and amplifies the magnitude of the R_{ex} term for residues initially assigned to model 3. At the final value of τ_c, 58% of the spins require an exchange term for an adequate fit. Moreover, inclusion of R_{ex} is accompanied by a reduction in the value of the order parameter for residues requiring the R_{ex} term (e.g. residues 23–44, Figure 2). Alternatively, residues requiring ns motions (fits to Model 5) exhibit an increased value of S^2 with decreasing τ_c (e.g. residues 67–69, Figure 2). Notably, order parameters are unaffected for residues fit by Models 1 or 2 for both values of τ_c (e.g. 76–86, Figure 2). In addition to the substantial increase in the number of exchange terms, 22 spins display statistically significant differences (at the 95% confidence level) in S^2 between the two data sets and these are generally associated with a change in model selection.

The behavior observed in the isotropic analysis of the experimental data can be rationalized by isotropic model-free fits to simulated relaxation data shown in Figure 3 (see figure legend for details). The simulated data are fit equally well (as shown by χ^2) by Model 3 with the correct τ_c (8.98 ns) or with a reduced τ_c (8.70 ns). The graph also shows the substantial errors in S^2 that result from neglect of anisotropic tumbling, which are discussed in detail in a later section. However, even when tumbling is isotropic, i.e. when $(3\cos^2\theta - 1)/2 = 0$ in Figure 3, failure to identify the correct τ_c leads to the assignment of erroneous motions and a change in S^2. In this case, an R_{ex} term is required to fit the data to compensate for the effective increase in T_2 at the lower, incorrect τ_c value. The issue for the present experimental data for DHFR is whether the observed exchange terms are genuine or are artifacts arising from an incorrect description of the diffusion tensor.

The diagnostic proposed by Tjandra et al. (1996) predicts that only six residues in DHFR exhibit exchange contributions. It is important to note, however, that the protocol of Tjandra et al. (1996) and other procedures based on T_1/T_2 ratios can break down in identifying R_{ex} terms for a protein that is dominated by ms–μs fluctuations. In such a case τ_c will be overestimated from the T_1/T_2 ratio, and most of the spins displaying smaller exchange terms will be fit to Model 1 during model selection. This was verified using simulated data for an isotropically tumbling protein ($\tau_c = 8.96$ ns) for which 70% of the residues had exchange terms ranging from 0.3 to 2.5 s^{-1}. The remaining residues were randomly assigned to one of the remaining four models. Errors for R_1, R_2, and NOE were set to 3%, 2.5% and 3.5%, respectively. Using the criteria of Tjandra et al. (1996), no R_{ex} terms were detected and the estimated τ_c from the T_1/T_2 ratio yielded an elevated τ_c value of 9.47 ns. Isotropic model-free analysis (at the elevated τ_c) fit 81% of the residues to Model 1 and only 11% of the residues to Model 3. Thus, the elevated τ_c value compensates for the exchange contributions to T_2 and most residues with genuine R_{ex} terms are described by the simplest model.

Thus, model-free analyses using the simulated data demonstrate that inaccurate description of the diffusion tensor (even for isotropic tumbling) gives rise to erroneous motions. For anisotropic tumbling the diffusion tensor can be calculated from the dependence of T_1 and T_2 data on the angles of the NH bond vectors relative to the axes of the diffusion tensor (Brüschweiler et al., 1995; Tjandra et al., 1995a; Zheng et al., 1995; Mackay et al., 1996; Lee et al., 1997). However, it is essential to exclude residues exhibiting slow motions from these calculations to obtain an accurate diffusion tensor (Lee et al., 1997; Kroenke et al., 1998). Novel NMR experiments and procedures have appeared attempting to detect slow motions (Akke et al., 1996, 1998; Zinn-Justin et al., 1997; Fushman and Cowburn, 1998; Fushman et al., 1998, 1999; Kroenke et al., 1998; van Tilborg et al., 1999; de Alba et al., 1999), but these require additional relaxation data, which can be time-consuming to acquire, and require highly stable samples. Additionally, procedures have been developed for improving the estimation of τ_c (Mandel et al., 1996; Lee et al., 1997; Yao et al., 1998), but these largely neglect the effects of rotational diffusion anisotropy. The COPED analysis provides a simple procedure for identifying slow motions in the presence of anisotropy to help better define the diffusion tensor and corroborate or refute model-free results. The procedure requires only T_1 and T_2 data, and therefore places no extra demands on sample stability. Additionally, since the diffusion tensor determined from COPED is insensitive to the relaxation data, it represents an independent procedure for confirming the experimentally determined diffusion tensors and for detecting motions.

Identifying genuine motions in proteins that tumble anisotropically using COPED

Table 1 reports the predicted degrees of anisotropy for the open, closed and occluded conformations of DHFR based on hydrodynamic calculations using the

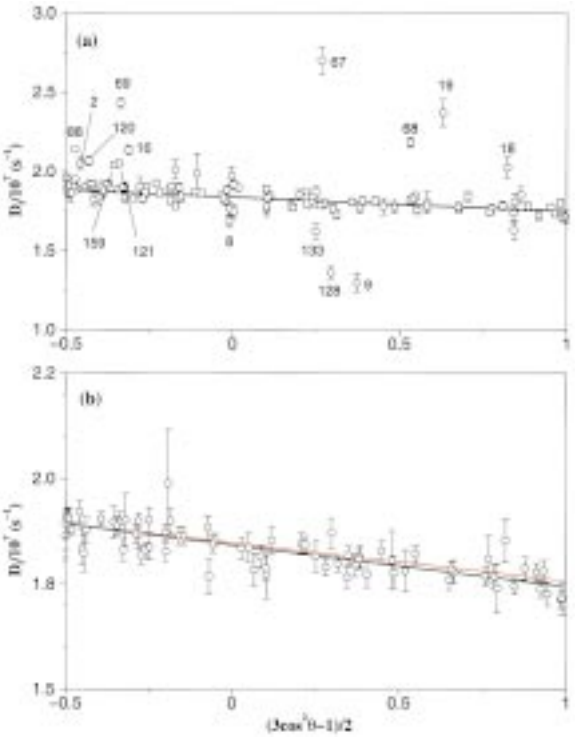

Figure 4. Graphical representation of the COPED analysis for the DHFR–folate–DHNADPH complex. (a) Diffusion coefficients derived from hydrodynamic modeling using the program MASH are plotted as a function of $(3\cos^2\theta - 1)/2$ (solid line). Experimental diffusion coefficients, $D_{i(exp)}$, calculated from the T_1/T_2 ratio are shown as open circles. The values of θ were obtained after rotating the structural coordinates (1rx2 in this example) to the principal axis frame of the diffusion tensor determined using MASH. Residues identified as having slow motions fall above and below the predicted diffusion tensor for ns and ms–μs timescales, respectively. (b) The black line shows diffusion coefficients determined from the diffusion tensor calculated from experimental relaxation data, for residues identified as undergoing fast motions by COPED, using the program quadric_diffusion (Lee et al., 1997). The diffusion coefficients predicted from the MASH analysis are shown for comparison (red line). $D_{i(exp)}$ values for NH bond vectors exhibiting fast motions are represented by open circles.

program MASH. The predicted linear relationship between the D_i and $(3\cos^2\theta - 1)/2$ (Equation 3), assuming axially symmetric rotational tumbling, is illustrated graphically in Figure 4a. (D_i values derived from the coordinates for the closed conformation, 1rx2, are plotted. Similar results were obtained for coordinates representing the open and occluded conformations.) The experimental values of D_i ($D_{i(exp)}$) are also shown in Figure 4a for values of θ determined from the hydrodynamic calculations.

The agreement of the relaxation parameters predicted from hydrodynamic calculations and the experimental data is excellent (Figure 4a, Table 1) and clearly indicates that the prevalent slow timescale (R_{ex}) motions required to describe the relaxation data in the isotropic model-free analysis are incorrect. Additionally, the relaxation data are accurately described by the angle θ for the majority of spins, justifying the inclusion of such data as restraints in structural calculations for residues that are known to undergo fast motions (Tjandra et al., 1997; Cordier et al., 1998). Indeed, the good agreement for the majority of residues indicates that the ternary DHFR complex studied in this paper does not differ considerably in solution from the X-ray coordinates, and vindicates their use as input structures in the following model-free analyses. Figure 4a can be used to distinguish genuine motions from the effects of anisotropy, since the linear relationship described in Equation 3 only holds true for residues undergoing very fast motions. Thus residues with D_i values that lie above the predicted line are likely to exhibit motions on the ps–ns timescale whereas values below the predicted line will have R_{ex} terms. In Table 1 we list residues exhibiting $\eta_i^2 > 6$ for all three sets of DHFR coordinates and use this criterion to identify slow motions (Note that the value of η_i^2 is system dependent and does not allow for a general cutoff value to be recommended. A more detailed discussion is presented later.) The COPED analysis predicts that only eight to nine residues in the ternary DHFR–folate–DHNADPH complex exhibit motions on the ms–μs timescale. Importantly, repeating the COPED procedure after excluding the slow motions identified above did not alter the C^α bead radius or the degree of diffusion, although the value of Γ was substantially decreased.

The excellent agreement for the experimental and predicted local diffusion coefficients also indicates that the relaxation data are not significantly influenced by site-specific differences in the CSA (Fushman and Cowburn, 1999).

The COPED procedure generally predicts the same residues with internal motions, irrespective of the coordinate set used. This reflects the similar backbone structures and hence similar orientation of NH bond vectors. The few discrepancies observed can be attributed to small differences in the X-ray coordinates. Significantly, residues comprising regions exhibiting the largest structural differences, i.e. residues in loop 1 (16,18,19) and the βF-βG loop (120,121) are predicted to undergo large-amplitude ns motions for all three sets of coordinates. It is unlikely, therefore, that the different orientations for these residues in the three

structure coordinates will bias model selection in the anisotropic model-free calculations. In Figure 4a we have labeled residues that exhibit extremely high η_i^2 values and which are therefore unlikely to be assigned an erroneous motion due to inaccuracies inherent in the hydrodynamics calculations.

Excluding the formation of aggregates using COPED

Formation of dimers or higher aggregates can lead to an increase in the rotational correlation time (see e.g. Farrow et al., 1994; Fushman et al., 1997; Fairbrother et al., 1998) and can adversely affect the model-free analysis (Schurr et al., 1994; Fushman et al., 1997). COPED clearly excludes the presence of a monomer–dimer equilibrium or higher aggregates which significantly affect the relaxation data in the present DHFR complex, since the formation of aggregated species would alter the hydrodynamic properties of the protein and it would not be possible to fit the experimental relaxation data to Equation 3 based on the hydrodynamic properties of the monomer coordinates.

Diffusion tensor refinement using quadric_diffusion

The diffusion parameters for the three X-ray coordinate sets calculated from experimental T_1/T_2 ratios using the quadric_diffusion program are shown in Table 3. Residues exhibiting slow motions were identified by COPED and excluded from this calculation. Figure 4b plots $D_{i(exp)}$ versus $(3\cos^2\theta - 1)/2$ for NH bond vectors exhibiting fast motions and shows that the bond vector orientations are uniformly distributed and can therefore be expected to accurately define the diffusion tensor. The diffusion tensor determined from quadric_diffusion does not differ significantly from that obtained using COPED (Figure 4b), and is best described by an axially symmetric diffusion tensor with $D_{||}/D_{\perp}$ ranging from 1.17 to 1.18 and a value of $1.84 \times 10^7\ s^{-1}$ for D_{iso} ($\tau_c = 9.05$ ns) (Table 3).

The degree of anisotropy from quadric_diffusion is virtually identical for all three coordinate sets, as indeed are the statistics of the fits. This reflects the similarity of the orientation of the NH vectors for the three structures and the fact that the largest structural differences between them are in regions which undergo motions on the ns timescale and which were therefore omitted from the calculations. If residues with slow motions identified from COPED are included in the quadric_diffusion calculation (final rows of Table 3), a significantly higher diffusion anisotropy of $D_{||}/D_{\perp} = 1.28$ is calculated, resulting in selection of erroneous motional models in subsequent model-free analyses. In contrast, COPED yielded identical diffusion tensors for relaxation data including and excluding slow motions (see above). This demonstrates a major advantage of using the COPED analysis to complement direct methods based on T_1/T_2 to determine the diffusion tensor. Firstly, COPED identifies slow motions which are important to exclude when determining the diffusion tensor from T_1/T_2 methods. Secondly, COPED serves as an independent method to assess the accuracy of the T_1/T_2-derived diffusion tensor. When large discrepancies arise between the two diffusion tensors, the experimenter must carefully assess the data. For example, differences can occur due to the formation of dimers or higher aggregates, the presence of extensive slow motions or even differences in the structural coordinates and the solution structure, all of which can be detrimental to model-free analysis.

Effects of complete anisotropy

The degree of complete anisotropy (D_{xx}/D_{yy}) predicted from hydrodynamic analysis (Table 1; $D_{xx}/D_{yy} \sim 1.06$) differs from the values calculated from quadric_diffusion when slow motions are excluded from the calculation (Table 3; $D_{xx}/D_{yy} \sim 1.02$). Moreover, F-testing indicates that an axially symmetric diffusion model best describes the relaxation data. This is not surprising, since the spins included in fitting the diffusion tensor with quadric_diffusion were chosen based on their fits to Equation 3, which assumes axially symmetric diffusion. It has been reported that degrees of anisotropic diffusion as low as $D_{xx}/D_{yy} = 1.05$ can be detected when the relaxation data is of high quality (Lee et al., 1997). In the principal axis system of the diffusion tensor for complete anisotropy, D_i is dependent on a second angle, ϕ, defined as the position of the NH vector on the x-y plane relative to the x-axis:

$$D_i = D_{iso} - \frac{(3\cos^2\theta - 1)\left(2D_{zz} - \left[D_{yy} + D_{xx}\right]\right)}{12} - \frac{\sin^2\theta\cos 2\phi\left(D_{xx} - D_{yy}\right)}{4} \quad (4)$$

where $D_{iso} = (D_{zz} + D_{xx} + D_{yy})/3$. The completely anisotropic component of the diffusion tensor ($D_{xx} - D_{yy}$) is dependent on the function $\sin^2\theta\cos 2\phi$. Figure 5a shows the effects of complete anisotropy on D_i for ϕ values of 0, 45 and 90° for anisotropic rotational diffusion of DHFR ($D_{iso} = 1.85 \times 10^7\ s^{-1}$, $2D_{zz}/(D_{xx} + D_{yy}) = 1.19$, $D_{xx}/D_{yy} = 1.05$) (see Table 4 and following section). When $\theta = 0°$, the effects of complete

Table 3. Diffusion parameters for X-ray coordinates of DHFR from ^{15}N relaxation data ($\eta_i^2 < 6$)[a]

	D_{iso} (10^{-7} s^{-1})	$2D_{zz}/(D_{xx}+D_{yy})$	D_{xx}/D_{yy}	θ (rad)[b]	φ (rad)[b]	ψ (rad)[b]	χ^2	F
1rx2.pdb[c]								
Isotropic[d]	1.84±0.01						392	
Axial[e]	1.84±0.01	1.18±0.01		1.46±0.04	4.81±0.03		81	97
Anisotropic[f]	1.84±0.01	1.18±0.01	1.02±0.01	1.46±0.10	−1.66±1.20	−0.08±0.52	79	0.94
1ra2.pdb[bg]								
Isotropic[d]	1.83±0.01						379	
Axial[e]	1.84±0.01	1.18±0.01		0.11±0.03	5.58±0.33		93	79
Anisotropic[f]	1.84±0.01	1.18±0.01	1.02±0.01	0.11±0.03	−0.76±0.37	−0.70±0.75	91	0.99
1rx7.pdb[bh]								
Isotropic[d]	1.84±0.01						400	
Axial[e]	1.84±0.01	1.17±0.01		1.61±0.04	4.80±0.04		102	76
Anisotropic[f]	1.84±0.01	1.17±0.01	1.01±0.01	1.53±0.05	1.65±1.52	1.45±1.21	99	1.03
1rx2.pdb[i]								
Isotropic[d]	1.88±0.01						2564	
Axial[e]	1.87±0.01	1.29±0.01		1.65±0.03	4.78±0.02		1559	24
Anisotropic[f]	1.87±0.01	1.27±0.01	1.09±0.01	1.65±0.05	−1.51±0.87	0.39±0.03	1495	2.4

[a]NH spins undergoing fast motions were identified by COPED. Only residues with $\eta_i^2 < 6$ were included in these fits.
[b]The angles θ, φ and ψ define the orientation of the diffusion tensor with respect to the coordinate frame of the inertia tensor.
[c]Values of $D_{i(exp)}$ for 80 residues were fit using the local diffusion approach.
[d]$D_{iso} = D_{zz} = D_{xx} = D_{yy}$.
[e]$D_{iso} = (2D_\perp + D_{||})/3$, $D_{||} = D_{zz}$, $D_\perp = D_{xx} = D_{yy}$, $D_{||}/D_\perp = 2D_{zz}/(D_{xx}+D_{yy})$.
[f]$D_{iso} = (D_{zz} + D_{xx} + D_{yy})/3$.
[g]Values of $D_{i(exp)}$ for 81 residues were fit using the local diffusion approach.
[h]Values of $D_{i(exp)}$ for 82 residues were fit using the local diffusion approach.
[i]$D_{i(exp)}$ values for all 115 NH spins (including residues undergoing slow motions).

Table 4. Diffusion parameters for X-ray coordinates of DHFR from ^{15}N relaxation data ($\eta_i^2 < 15$)[a]

	D_{iso} (10^{-7} s^{-1})	$2D_{zz}/(D_{xx}+D_{yy})$	D_{xx}/D_{yy}	θ (rad)[b]	φ (rad)[b]	ψ (rad)[b]	χ^2	F
1rx2.pdb[c]								
Isotropic[d]	1.85±0.01						638	
Axial[e]	1.85±0.01	1.19±0.01		1.61±0.03	1.60±0.03		184	77
Anisotropic[f]	1.85±0.01	1.19±0.01	1.05±0.01	1.59±0.04	1.60±1.41	−0.10±0.17	165	5.2
1ra2.pdb[g]								
Isotropic[d]	1.85±0.01						596	
Axial[e]	1.85±0.01	1.19±0.01		0.09±0.03	5.82±0.34		187	67
Anisotropic[f]	1.85±0.01	1.18±0.01	1.04±0.01	0.07±0.03	−0.51±0.48	−0.50±0.68	173	3.6
1rx7.pdb[h]								
Isotropic[d]	1.85±0.01						581	
Axial[e]	1.85±0.01	1.18±0.01		1.56±0.03	4.73±0.04		176	70
Anisotropic[f]	1.85±0.01	1.18±0.01	1.05±0.01	1.56±0.04	−1.56±1.52	−1.46±1.40	160	4.4

[a]NH spins included in the analysis were identified from COPED. Residues with $\eta_i^2 < 15$ were included in these fits.
[b]The angles θ, φ and ψ define the orientation of the diffusion tensor with respect to the coordinate frame of the inertia tensor.
[c]Values of $D_{i(exp)}$ for 98 residues were fit using the quadric_diffusion approach.
[d]$D_{iso} = D_{zz} = D_{xx} = D_{yy}$.
[e]$D_{iso} = (2D_\perp + D_{||})/3$, $D_{||} = D_{zz}$, $D_\perp = D_{xx} = D_{yy}$, $D_{||}/D_\perp = 2D_{zz}/(D_{xx}+D_{yy})$.
[f]$D_{iso} = (D_{zz} + D_{xx} + D_{yy})/3$.
[g]Values of $D_{i(exp)}$ for 96 residues were fit using the quadric_diffusion approach.
[h]Values of $D_{i(exp)}$ for 96 residues were fit using the quadric_diffusion approach.

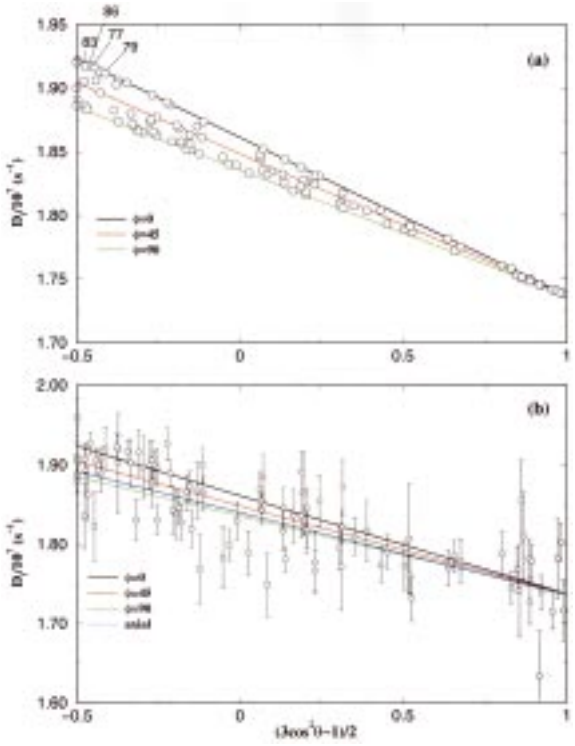

Figure 5. (a) The effects of complete anisotropy on D_i for ϕ values of 0°, 45° and 90° (black, red and green lines, respectively) and anisotropic rotational diffusion defined by: $D_{iso} = 1.85 \times 10^7\ s^{-1}$, $2D_{zz}/(D_{xx} + D_{yy}) = 1.19$, $D_{xx}/D_{yy} = 1.05$. Predicted D_i values derived from the quadric_diffusion fit (Lee et al., 1997) of the structural coordinates, 1rx2, to the completely anisotropic tensor (Table 4) are shown as circles. Spins exhibiting $\eta_i^2 < 15$ from COPED were included in the quadric_diffusion analysis. Residues in helix E (77–86) predicted to be sensitive to the effects of complete anisotropy are marked (see text). (b) Plot showing the experimental values of $D_{i(exp)}$ (circles) and a plot of D_i versus $(3\cos^2\theta - 1)/2$ from the axially symmetric diffusion tensor determined from quadric_diffusion (blue line). Note that the errors are generally much larger than the predicted effects to D_i from complete anisotropy.

anisotropy are negligible and Equation 4 reduces to the axially symmetric case. Complete anisotropy has the largest effect on D_i when $\theta = 90°$ and $\phi = 0°$ or 90°. When $\phi = 45°$, Equation 4 again reduces to Equation 3 and tumbling can be described by an axially symmetric diffusion tensor.

To compensate for possible errors introduced by complete anisotropy in identifying fast motions using COPED, we relaxed the criteria of the fits so that spins exhibiting $\eta_i^2 < 15$ were included in fitting the diffusion tensor. Subsequent analysis with quadric_diffusion shows that the data are now best described by a completely anisotropic diffusion tensor (Table 4). Indeed, the statistical F-test indicates that the completely anisotropic tensor for values of $\eta_i^2 < 15$ better describes the data than the axially symmetric tensor for values of $\eta_i^2 < 6$ ($F \sim 5$).

Local D_i values predicted from fitting the completely anisotropic diffusion tensor for DHFR (coordinates 1rx2) using quadric_diffusion on spins identified using COPED with a cutoff of $\eta_i^2 < 15$ indicate that a number of residues are expected to be influenced by complete anisotropy (Figure 5a). For example, NH vectors comprising the E-helix (77–86), marked on Figure 5a, are aligned predominantly perpendicular to the principal diffusion axis and display ϕ values close to 0, and are thus sensitive to the small D_{xx}/D_{yy} component of 1.05 (Table 4). Small uncertainties (~ 0.065 ns on average for τ_{ci}) are associated with the spins in helix E, which is lower than the change in τ_{ci} predicted from the D_{xx}/D_{yy} component of the diffusion tensor ($\Delta\tau_{ci} \sim 0.09$ ns). Accordingly, these residues are expected to exhibit elevated values for D_i due to complete anisotropy, explaining the assignment of ps timescale motions to these residues when $\eta_i^2 > 6$ is used to determine motions in COPED (Table 1). For most residues, however, the uncertainty of the measurements (~ 0.13 ns on average for τ_{ci}) is greater than the effects of complete anisotropy on the relaxation data (Figure 5b). Thus, the effects of complete anisotropy are not expected to be large when an axially symmetric diffusion tensor is assumed. Indeed, inclusion of residues sensitive to complete anisotropy propagates only minimal changes in the axially symmetric diffusion tensors (Tables 3 and 4) and is unlikely to substantially affect the axially symmetric model-free analysis, as shown in the following section.

Model-free analysis assuming axially symmetric rotational diffusion anisotropy

Model selection was performed for the three DHFR coordinate sets using the axially symmetric diffusion tensors for the first three rows in Table 3. We found that the relaxation data for a number of NH spins could not be adequately described by any of the five models using an $\alpha = 0.05$ critical value of the χ^2 distribution. Most of these spins exhibited lower than average uncertainties for the relaxation data. Model selection for these residues was therefore repeated using the average uncertainty values calculated from all spins. It was now possible to fit most of the spins to one of the five models. Model selection (determined from F-testing) was not altered in any of the cases and the parameters

describing the internal motions were not significantly changed. It is probable that the uncertainties in the relaxation data for these residues were underestimated. Spins expected to be sensitive to fully anisotropic tumbling (e.g. helix E) could not be described by any model unless the uncertainties were relaxed. In the following analyses, the original uncertainty values were used. To determine how the model-free analysis is affected by the residues that are sensitive to the effects of complete anisotropy, we fitted the diffusion tensor simultaneously with the internal motional parameters using two protocols. In the first method (a) we included only those spins that gave acceptable fits to models 1 to 4, i.e. within the $\alpha = 0.05$ critical value of the χ^2 distribution. For the second procedure (b), all spins (regardless of whether or not they gave acceptable fits) except those described by Model 5 were used to fit the diffusion tensor. For both protocols, the original uncertainty values were used. Procedure (a) was applied to all three coordinate sets. Coordinates for 1rx2 were used for procedure (b).

Model selection and the parameters describing the final optimized diffusion tensors for procedures (a) and (b) are summarized in the first and last rows, respectively, of Table 5. Procedure (b) required 2 cycles of model selection to obtain a stable diffusion tensor, and therefore the tensor differs slightly from that obtained in procedure (a) which remained at the initial value. Figure 6 indicates that the effects of complete anisotropy are responsible for the observed differences in the axial diffusion tensors. For procedure (b) spins in helix E (residues 77–86), which are influenced by completely anisotropic tumbling (Figure 5a), are included and their elevated D_i values in combination with their small uncertainties are responsible for the larger degree of axial anisotropy (Figure 6b). Interestingly, these residues do not require different motional models to describe the data, although the quality of the fits is slightly improved using procedure (b). Despite the differences in the diffusion tensor between procedures (a) and (b), model selection is only minimally affected (Table 5, first and last rows). In general, procedure (b) requires some extra small R_{ex} terms (<0.6 s^{-1}) for residues 28, 35, 57 and 147 to fit the data; this can be rationalized graphically by the increased gradient displayed by the tensor for procedure (b) (Figure 6b). This plot also indicates that the spins most likely to require a change in model to describe the data will have θ values approaching 90°. This is demonstrated for spins 35 and 57 (θ values of 60° and 70°, respectively), which require small R_{ex} terms to

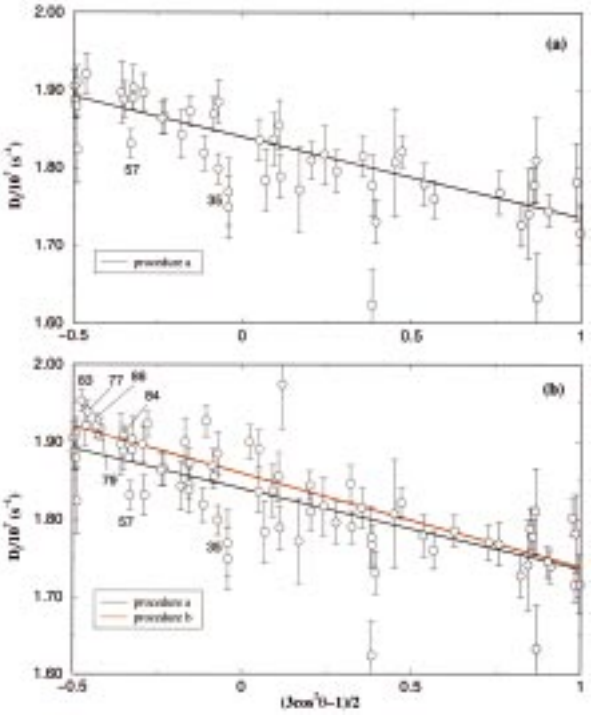

Figure 6. (a) Plot (black line) of D_i versus $(3\cos^2\theta - 1)/2$ for the optimized axially symmetric diffusion tensor determined using procedure a (see text for details). The experimental diffusion coefficients used to determine the tensor in the final step of the axially symmetric model-free analysis are shown as circles. (b) Plot (red line) of D_i versus $(3\cos^2\theta - 1)/2$ for the optimized axially symmetric diffusion tensor determined using all spins described by Models 1 to 4 (procedure b). The plot obtained using procedure a is included (black line) for comparison. The inclusion in procedure b of residues with small uncertainties that are sensitive to completely anisotropic tumbling (e.g. residues 77–86 are marked) is the probable origin of the observed differences between the tensors. Residues 57 and 35 requiring an extra R_{ex} term to fit the data in procedure b are shown (see text).

fit the tensor using procedure (b) (Figure 6). Values of S^2 are virtually unchanged; only the four residues requiring extra exchange terms exhibit a statistically different S^2 value at the 95% confidence level.

Comparison of different structural coordinates

Differences in model selection obtained using the three different coordinate sets for the DHFR complex are summarized in Table 5. The diffusion tensor (Table 3), model selection (Table 5), and model-free parameters (data not shown) are largely unaffected by the choice of X-ray structure. Changes in S^2 resulting from the use of different coordinate sets are so small that they are within the uncertainties (assuming 95% confidence in the data) for the majority of

Table 5. Summary of model selection for axially symmetric model-free analyses[a]

PDB file	D_{iso} (10^{-7} s^{-1})[b]	D^b_{rat}	S^2	S^2, τ_e	S^2, R_{ex}	S^2, τ_e, R_{ex}	S^2_f, S^2_s, τ_s
1rx2[c]	1.84 (1.84)	1.18 (1.18)	68	22	8	6	11
1ra2[c]	1.84 (1.84)	1.18 (1.18)	71	20	6	7	11
1rx7[c]	1.84 (1.84)	1.17 (1.18)	69	21	10	4	11
1rx2[d]	1.86 (1.84)	1.21 (1.18)	65	22	11	7	11

[a] $D_{iso} = (2D_\perp + D_{||})/3$, $D_{rat} = D_{||}/D_\perp$, $D_{||} = D_{zz}$, $D_\perp = D_{xx} = D_{yy}$, $D_{||}/D_\perp = 2D_{zz}/(D_{xx} + D_{yy})$.
[b] Final value after optimization; initial value in parentheses.
[c] Determined using protocol (a).
[d] Determined using protocol (b).

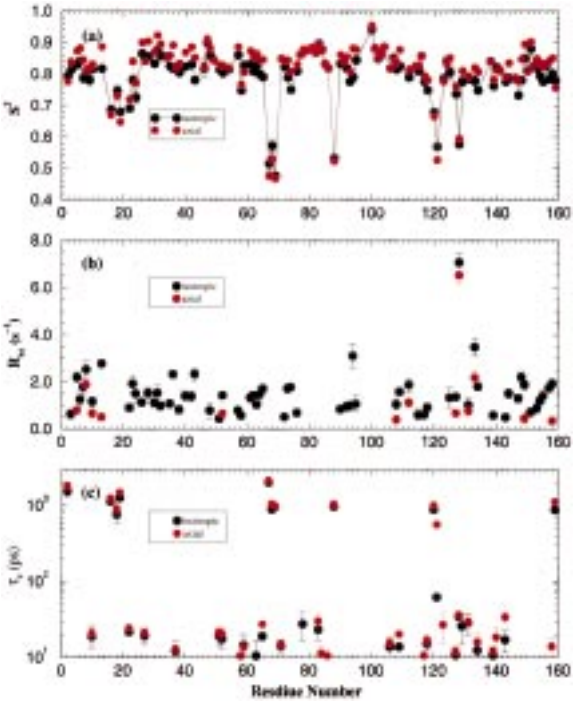

Figure 7. Comparison of the internal motional parameters determined assuming an isotropic (at the final τ_c, 8.70 ns, black circles) and axially symmetric (procedure a, red circles) model-free spectral density function. Note the substantial increase in exchange terms required to fit the data assuming an isotropic tumbling and the differences in S^2 between the two analyses.

residues. The only exceptions are some of the residues (18, 19, 22) in loop 1. Loop 1 undergoes the largest conformational changes between the open, closed, and occluded structures, resulting in differences in θ for the NH bond vectors in this region. For example, $\Delta\theta$ between coordinate sets 1rx7 and 1ra2 for the NH of I18 is 49.5° and this is associated with a change in S^2 of 0.05. Despite the large variations in θ amongst the X-ray structures, these residues consistently require the same model (Model 5) to describe the data. Thus, we are confident that the large-amplitude ns timescale motions are genuine and are not artifacts of the value of θ.

Comparison of model-free analyses assuming isotropic and axially symmetric diffusion tensors

Figure 7 compares the internal motional parameters for DHFR determined from model-free analyses assuming isotropic and axially symmetric rotational diffusion tensors. Clearly, the assumption of isotropic rotational diffusion for the ternary DHFR complex introduces a large number of erroneous motional parameters, especially in R_{ex}. Statistically significant differences (at the 95% confidence level) for S^2, R_{ex} and τ_e were observed for 57, 60 and 12 residues, respectively. A total of 58 spins (~50% of the assigned residues) were fit by different models in the two analyses. This is summarized in Figure 8, where the model selections for the isotropic and axially symmetric model-free analyses are mapped onto the coordinates of DHFR (oriented so that the symmetry axis of the diffusion tensor is vertical). The backbone NH bond vectors are also shown. The introduction of erroneous R_{ex} terms is closely related to the orientation of the NH vector with respect to the principal axis of the diffusion tensor (Figure 8). For example, the NH vectors of the B helix are aligned predominantly parallel to the principal diffusion axis and largely require R_{ex} terms to fit the data under the assumption of an isotropic diffusion model. The influence of anisotropic rotational diffusion anisotropy on relaxation data is well known (Schurr et al., 1994; Tjandra et al., 1995b; Luginbühl et al., 1997). In published studies, however, the effects of incorrectly assuming isotropic tumbling in model-free analysis have been minor: S^2 was minimally affected and changes in motional models were detected for only a small proportion of the residues (Tjandra et al., 1995b; Luginbühl et al., 1997; Gagné et al., 1998). The analysis presented here is the first case

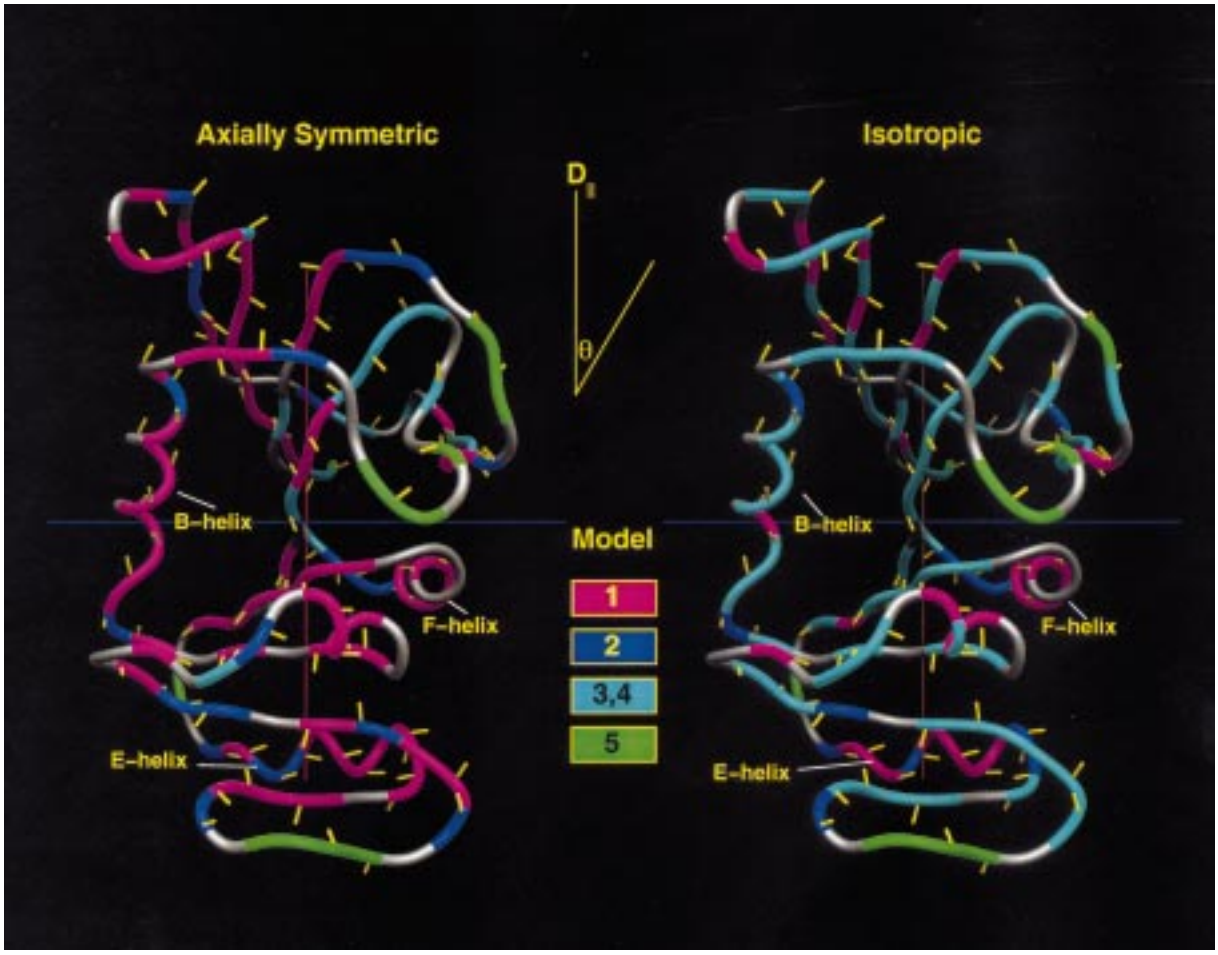

Figure 8. Summary of the model selections assuming isotropic and axially symmetric model-free spectral density functions. Motional models are mapped onto the X-ray structure of DHFR (1rx2) oriented into the axially asymmetric diffusion tensor coordinate frame. The orientation of the NH vectors for each analyzed spin is also shown. Residues requiring R_{ex} terms (Models 3 and 4) are colored cyan.

in which the neglect of anisotropic tumbling in the model-free spectral density function results in major errors in the assignment of motional models: significantly, 52 residues (i.e. 45%) are assigned erroneous R_{ex} terms. The number of erroneous exchange terms is surprising, considering the small degree of anisotropy exhibited by DHFR. Furthermore, the NH bond vectors are aligned predominantly perpendicular to the principal diffusion axis (Figure 4) and are predicted to introduce motional errors on the ps–ns timescales assuming isotropic motion (Schurr et al., 1994). We note, however, that this prediction assumes that the correct value of τ_c is used for model selection. In the case of DHFR, the effective τ_c is significantly reduced during the optimization stage when an isotropic model is used, due to the numerous NH vectors aligned perpendicular to the symmetry axis (33 NH vectors have θ angles between 70° and 90°, only 18 NH vectors have a value of θ between 0° and 30°).

Figure 3 shows the effects on S^2, R_{ex} and χ^2 of fitting relaxation data influenced by anisotropic rotational diffusion at an incorrect τ_c to the isotropic tensor model-free analysis. Relaxation data were simulated assuming axial asymmetry ($D_{||}/D_{\perp} = 1.30$) and $S^2 = 0.8$, and no internal motions (further details are given in the figure legend). The horizontal line in panel c of Figure 3 indicates an acceptable fit. This figure readily explains the trends observed for the isotropic model-free analysis of the DHFR ternary complex. Thus, at the correct τ_c (solid circles), the expected influence of anisotropy is observed: values of θ approaching 0° require R_{ex} terms to fit the data (the value of which increases with a decrease in θ), and as $\theta \rightarrow 90°$, ns timescale motions are required

to fit the data[1]. At the decreased value of τ_c, spins at intermediate values of θ that were originally fit by Model 1 now require an exchange term to compensate for an effective decrease in T_2 and spins initially assigned erroneous R_{ex} terms require even larger exchange terms to fit the data. Spins with θ close to 90° are now adequately fit by Model 1 at the reduced value of τ_c. This explains the lack of ns–ps motions required to fit for our experimental data using isotropic model-free analysis, despite the numerous spins with θ close to 90° (e.g. the E- and F-helices, Figure 8) and also explains the unexpectedly large number of exchange contributions.

A relationship between S^2 and R_{ex} is also evident from the simulated data of Figure 3. The deviation of S^2 from the true value ($S^2 = 0.8$) increases as θ approaches 0 when the data are fitted using a small, incorrect value of τ_c (Figure 3a). Further, this error is greatly amplified when an exchange term is included to fit the data. We note that the quality of fits in an isotropic analysis is significantly improved by the inclusion of an R_{ex} term when the value of τ_c is underestimated (Figure 3c) and Model 3 (S^2 plus R_{ex}) is therefore selected in the model-free analysis after F-testing. As a consequence, significant errors can be introduced into S^2. Comparison of the isotropic and axially symmetric model-free analyses (Figure 7) clearly shows this dependence of S^2 on R_{ex} (we note a similar dependence for residues fit to Model 5). The 10% trimmed weighted mean difference in S^2 for these residues is 0.036, with differences as large as 0.06–0.08 observed for spins aligned parallel to the principal diffusion tensor axis. Conversely, spins assigned to Model 1 and Model 2 in both analyses do not exhibit marked changes in S^2; the 10% trimmed weighted mean difference in S^2 for these residues is 0.0037, which is well within the uncertainties of the experiments. Theoretically, S^2 and R_{ex} should not be related since the spectral density function does not contain any information on motions slower than the rotational correlation time (Lipari and Szabo, 1982a,b). In practice, however, an effective spectral density ($J(0)_{eff}$) is implicitly fit during the model-free analysis which is increased by exchange terms, $J(0)_{eff} = J(0)_{true} + R_{ex}$ (Peng and Wagner, 1995). A decrease in τ_c induces a decrease in the 'true' $J(0)$ and thus an increase in $J(0)_{eff} - J(0)_{true}$ and thus results in a greater need for an exchange contribution to fit the data.

The errors in S^2 that arise from the inappropriate assumption of isotropic tumbling are important when detailed analyses of relaxation data are performed. For example, changes in S^2 have been used to estimate the change in Gibbs free energy ($\Delta\Delta G$) between two states (Akke et al., 1993). For DHFR, the differences in S^2 between model-free fits for isotropic and anisotropic tumbling models correspond to a total difference in ΔG of 8.3 kcal/mol.[2] In other words, incorrect assumption of an isotropic diffusion tensor would lead to large errors in thermodynamic parameters. Clearly in the present analysis, the greatest consequence of anisotropic rotational tumbling on the isotropic model-free analysis is that τ_c is underestimated. It is this incorrect value of τ_c that gives rise to erroneous model-free parameters.

Comparison of axially symmetric model-free and COPED analyses for identifying motions.

The COPED (Table 1, Figure 4a) and axially symmetric model-free analyses (Figures 7–9) show excellent agreement for identifying slow motions. For ns–ps motions, there are only two discrepancies between the analyses assuming that values of $\tau_e > 30$ ps in the model-free analysis are reliable (Palmer et al., 1996) and using a cutoff above 15 for η_i^2 in the COPED analysis. These discrepancies are residues 128 and 129, which were shown to exhibit both ns–ps and ms–μs motions in the axially symmetric model-free analysis. All residues with $R_{ex} > 0.5\ s^{-1}$ in the axially symmetric model-free analysis were identified by the COPED procedure when a cutoff value of $\eta_i^2 > 6$ was used. A lower η_i^2 value is required to identify ms–μs motions, probably due to the effects of complete anisotropy which increase the degree of axial anisotropy in the model-free analysis.

The value of η_i^2 is highly dependent on the errors associated with the relaxation data (e.g. smaller values of η_i^2 are associated with larger errors), which therefore makes it impossible to recommend a standard cutoff for η_i^2 with which to identify slow motions. Moreover, possible errors introduced into the COPED procedure, for example from differences in the X-ray and solution structures, possible effects of complete anisotropy (see above) and assumptions in the hydrodynamic modelling make the choice of η_i^2 system

[1] Note that at the correct τ_c the quality of fits is substantially worse for $\theta = 0°$ than $\theta = 90°$ (Figure 3c), implying it is more likely to erroneously fit ms–μs motions than ps–ns motions when the correct value of τ_c is used.

[2] $\Delta\Delta G = \Sigma - RT * \ln(1 - S^2_{iso}/1 - S^2_{anis})$ summed over all residues.

dependent and non-trivial. Our experience has shown it is prudent to visualise the results graphically to identify outliers and choose a value for η_i^2 accordingly. Alternatively, to account for the errors in the relaxation data a cutoff value of η_i^2 can be chosen from a weighted average, or trimmed weighted value of η_i^2. As an example, one standard deviation above the 5% trimmed weighted average for η_i^2 yielded a cutoff for η_i^2 of 7.4 for the present data, which did not alter the subsequent diffusion tensor and axially symmetric model-free analyses.

The excellent results obtained here with COPED have been mirrored for other protein systems in our laboratory, suggesting that the procedure can be generally applied to proteins where accurate structural coordinates are available, although testing on a wider range of protein systems is required. We also note that in the present analysis, the hydrodynamic calculations were performed with each residue represented by a single bead centred at the C^α position to minimize cpu time. Due to the excellent results obtained we did not explore other hydrodynamic modelling options, such as explicitly including all heavy atoms and water molecules around the protein, although it would be interesting to see how such modifications would affect the COPED analysis.

The fact that COPED relies on hydrodynamic modelling to obtain the diffusion tensor implies it will not be susceptible to errors introduced by slow motions or where the NH vectors are non-uniformly distributed about θ, which can occur from direct T_1/T_2 methods (Lee et al., 1997; Kroenke et al., 1998). In helical bundle proteins, for example the 16th spectrin repeat (Pascual et al., 1996, 1997), there is generally a non-uniform distribution of NH vectors (Figure 9a) such that the diffusion tensor cannot be accurately described using direct T_1/T_2 methods. For the 16th spectrin repeat (Figure 9a) the small number of residues that are not aligned parallel to the principal diffusion axis are in loop regions (33–38, 76–81) and exhibit motions (Pascual et al., 1996, 1997) which can further define an inaccurate diffusion tensor. Clearly, using averaged T_1/T_2 ratios to exclude motions and subsequently fit the diffusion tensor will lead to a substantially underestimated degree of diffusion, and additionally an underestimated value for τ_{ciso}. Application of a procedure such as COPED, which does not rely on relaxation data to define the diffusion tensor, is advantageous in defining slow motions and accurate rotational diffusion in these systems.

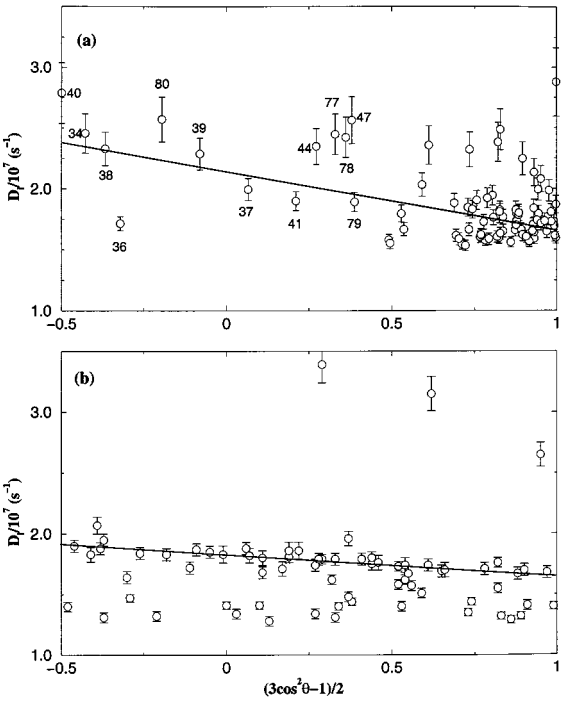

Figure 9. (a) COPED analysis for simulated relaxation data (shown as open circles). Data were simulated at 600 MHz for 70 NH spins undergoing axially symmetric rotational diffusion described by $D_{||}/D_\perp = 1.3$ and $\tau_c = 8.96$ ns. 50% of the spins were randomly assigned R_{ex} terms ranging from 0.5 to 7 s^{-1}, 35% were assigned to Model 1 (S^2) only. The remaining spins were assigned to Models 2 and 5. For each spin, a value of θ between 0 and 90° was randomly assigned. Errors associated with R_1, R_2 and NOE were set to 3%, 2.5% and 3.5%, respectively. (b) COPED analysis for a representative NMR structure for the 16th spectrin repeat (Pascual et al., 1996, 1997) (solid line). The best fit to the experimental relaxation data (open circles) was determined by minimizing Γ by altering the C^α bead radius.

We have shown in a previous section that COPED is less susceptible to defining an erroneous diffusion tensor than direct T_1/T_2 methods when residues undergoing slow motions are included. It is not clear, however, whether COPED can accurately define the correct diffusion tensor when the dynamics of a protein are dominated by slow motions. That COPED can reliably identify these motions for simulated relaxation data exhibiting axially symmetric anisotropic rotational diffusion and R_{ex} terms for 50% of the spins is demonstrated in Figure 9b (see figure legend for further details). The COPED analysis identified all 35 residues undergoing exchange (a low cutoff of $\eta_i^2 = 2$ can be used since the data were simulated). We note that the Tjandra method (1996) identified only 12 of the 35 R_{ex} terms present for these simulated data.

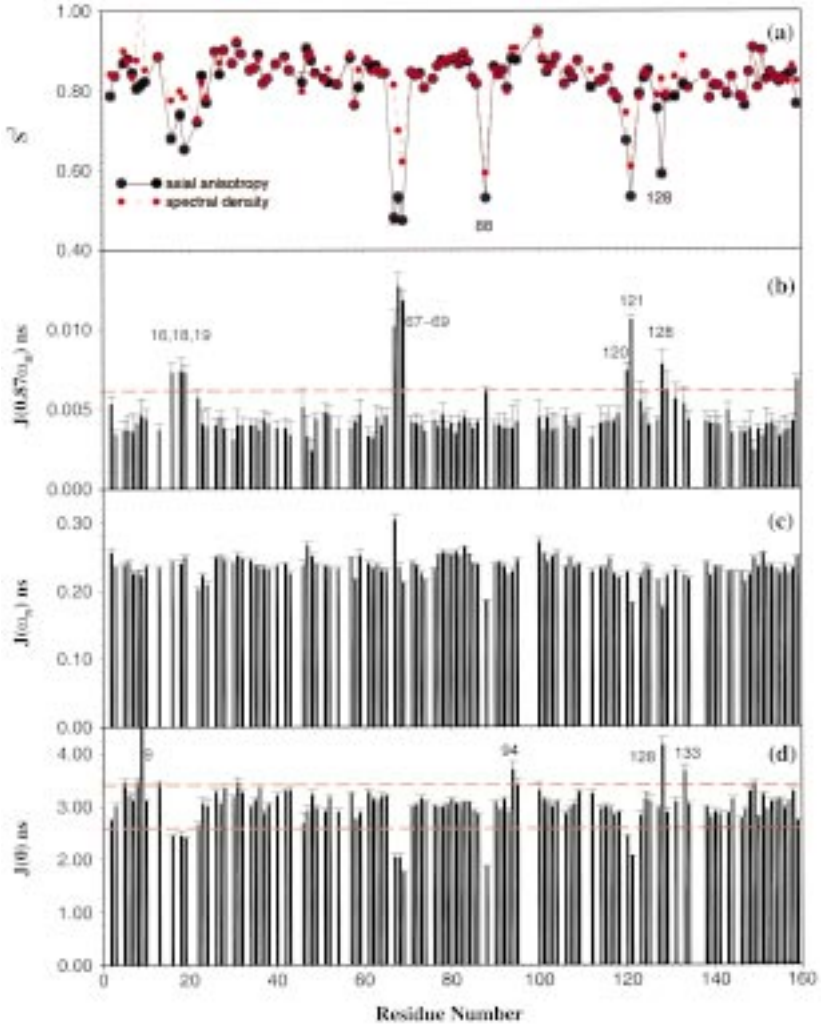

Figure 10. Values of (b) $J(0.87\omega_H)$, (c) $J(\omega_N)$ and (d) $J(0)$ derived from R_1, R_2 and NOE at 14.1 T using spectral density mapping. Panel (a) shows S^2 values determined from the axially symmetric model-free analysis (black circles) and by the spectral density mapping method (red circles). The red horizontal line is one standard deviation above the mean value in (b) and one standard deviation above and below the mean value in (d).

However, testing on experimental data sets will be required to ascertain whether COPED can identify the correct diffusion tensor for 'real' proteins exhibiting such pathological motions. Nevertheless, the fact that it is difficult to establish a single linear relationship, as in Figure 9b, is in itself a good indication that a substantial proportion of residues exhibit slow motions. Indeed, in this respect, COPED has successfully served one of its purposes, which is to identify motions, although not to specific residues. We can suggest some general guidelines based on our practical experience that can help to define the correct tensor, using the data in Figure 9b, and our experience with DHFR as an example. First, we note that it is unlikely that the slow motions will exhibit a linear relationship whose gradient coincides with that predicted from hydrodynamic modelling; thus, a larger Γ value is obtained when only residues undergoing exchange terms are included in the COPED analysis for the data in Figure 9b. This is because the value of D_{rat} is relatively insensitive to the value of the bead radius (e.g. D_{rat} is altered by 0.06 when the bead radius is altered from 2.2 to 3.2 Å in DHFR). In contrast, D_{iso} is dramatically altered by the bead radius (τ_{iso} is 9.05 ns and 5.64 ns for bead radii of 3.2 Å and 2.2 Å, respectively for DHFR). Thus, knowledge of the global correlation

time for the size of the protein under study will help in deciding a correct bead radius. For example, the τ_{ciso} obtained from attempting to fit only exchange residues in Figure 9b is 11.5 ns, which is 3.5 ns larger than the correct value. Finally, our practical experience indicates that a C^{α} bead radius of ~ 3.0 Å is usually required to give excellent fits for well-behaved proteins. This is a good initial estimate with which to commence the COPED procedure, and any large deviation from this value is unusual.

Reduced spectral density mapping

The values of $J(0)$, $J(\omega_N)$ and $J(0.87\omega_H)$ derived from R_1, R_2 and NOE at 14.1 T are presented graphically in Figure 10. The reduced spectral density analysis, which does not assume any model for the diffusion tensor, substantiates findings from the axially symmetric model-free analysis, both for residues exhibiting high frequency motions (characterized by low values of $J(0)$ and high $J(0.87\omega_H)$) and exchange contributions (based on $J(0)$ values larger than one standard deviation above the mean). It is tempting to assign an R_{ex} term to I94; however, its N-H is parallel to the principal diffusion axis and the spectral density analysis is sensitive to rotational diffusion, e.g. $J(0)$ can change by 0.276 ns for an axial symmetry of 1.3 ($S^2 = 0.8$, $\tau_e = R_{ex} = 0$) as a function of θ. This value is similar to the increase in $J(0)$ predicted for an R_{ex} of 1 s^{-1} (0.28 ns). Spins requiring both R_{ex} and τ_e contributions in the model-free analysis (residues 10, 52, 127, 131 and 158) affect $J(0)$ in opposing directions and thus show no obvious exchange contributions from the spectral density analysis.

The S^2 values obtained from the axially symmetric model-free analysis and reduced spectral density are very similar for all spins fit by motional Models 1 and 2, but differ significantly when higher motional models are involved (Figure 10a). We were able to show from simulated data that the error in S^2 originates in the spectral density mapping analysis (data not shown). This is due to the effects of slow motions (ns–ps and ms–μs) on the true $J(0)$ value, which need to be subtracted out to obtain a correct S^2, and the absence of information from $J(0.87\omega_H)$ which contains information on ps–ns motions. The same simulated data confirmed the excellent agreement observed in DHFR for S^2 values obtained by spectral density mapping and axially symmetric model-free analysis for residues described by Models 1 and 2. This suggests that comparison of S^2 values obtained by the two methods can be used to confirm that the correct diffusion tensor has been defined in the model-free analysis.

Conclusions

Dynamic information from NMR relaxation data is often used to provide insights into protein function. Many studies have reported motional properties at functionally relevant sites in proteins or used comparisons of S^2 values to measure changes in conformational entropy upon formation of a complex. For such applications to be valid, accurate and precise interpretation of relaxation data is required.

We have demonstrated that the moderate degree of anisotropy exhibited by the ternary DHFR complex ($D_{||}/D_{\perp} = 1.18$) introduces significant errors in the internal motional parameters extracted from the model-free analysis when rotational diffusion is assumed to be isotropic. Our results contrast with previous studies, which suggested that anisotropic rotational diffusion only marginally affects the selection of motional models and has little effect on the value of S^2. Assumption of isotropic tumbling in the model-free analysis of the ternary DHFR complex leads to the assignment of erroneous motions (on the ms–μs timescale) to 45% of the NH spins analyzed. In addition, this inappropriate assumption significantly changes the value of S^2 for spins fit to Models 3, 4 and 5. Deviations in S^2 as large as 0.08 were observed for NH spins parallel to the principal axis of the diffusion tensor. A detailed analysis of the data shows that anisotropic tumbling reduces the value of τ_c during the isotropic model-free analysis, due to the high quality of the relaxation data and the preponderance of NH vectors aligned perpendicular or nearly perpendicular to the principal diffusion axis. This in turn exaggerates the effects of anisotropy for the remaining spins.

A novel procedure, COPED, has been developed to distinguish genuine motions from the effects of rotational diffusion anisotropy. COPED represents a powerful method for defining the correct diffusion tensor from relaxation data and improving the accuracy of the subsequent model-free analysis. Motions identified from COPED show excellent agreement with motions identified from the anisotropic model-free analysis for the ternary DHFR complex. COPED is potentially applicable to any system for which a high-resolution structure is available, including systems where the orientational distribution of the NH vec-

tors is non-uniform and where there are extensive slow motions.

DHFR represents an extreme case in which neglect of anisotropic tumbling leads to serious errors in model selection and internal motional parameters (even in S^2) in the model-free analysis. If left uncorrected, such data can lead to misleading dynamic parameters that can hinder our understanding of the role of motions in biological processes.

Acknowledgements

We thank Dr. Ishwar Radhakrishnan for invaluable assistance, discussions and development of the program MASH and Drs. Stephen Benkovic, David Epstein, Paul Miller, Sergio Scrofani and Jane Dyson for helpful discussions. Dr. Arthur Palmer is thanked for providing the software Modelfree4.01, tmest and quadric_diffusion. This work was supported by grant number GM56879 from the National Institutes of Health.

References

Akke, M., Liu, J., Cavanagh, J., Erickson, H.P. and Palmer, A.G. (1998) *Nat. Struct. Biol.*, **5**, 55–59.

Akke, M. and Palmer, A.G. (1996) *J. Am. Chem. Soc.*, **118**, 911–912.

Akke, M., Brüschweiler, R. and Palmer, A.G. (1993) *J. Am. Chem. Soc.*, **115**, 9832–9833.

Barbato, G., Ikura, M., Kay, L.E., Pastor, A.W. and Bax, A. (1992) *Biochemistry*, **31**, 5269–5278.

Bracken, C., Carr, P.A., Cavanagh, J. and Palmer, A.G. (1999) *J. Mol. Biol.*, **285**, 2133–2146.

Brüschweiler, R., Liao, X. and Wright, P.E. (1995) *Science*, **268**, 886–889.

Cannon, W.R., Singelton, S.F. and Benkovic, S.J. (1996) *Nat. Struct. Biol.*, **3**, 821–833.

Clore, G.M., Driscoll, P.C., Wingfield, P.T. and Gronenborn, A.M. (1990b) *Biochemistry*, **29**, 7387–7401.

Clore, G.M., Szabo, A., Bax, A., Kay, L.E., Driscoll, P.C. and Gronenborn, A.M. (1990a) *J. Am. Chem. Soc.*, **112**, 4989–4991.

Cordier, F., Caffrey, M., Brutscher, B., Cusanovich, M.A., Marion, D. and Blackledge, M. (1998) *J. Mol. Biol.*, **281**, 341–361.

de Alba, E., Baber, J.L. and Tjandra, N. (1999) *J. Am. Chem. Soc.*, **121**, 4282–4283.

Epstein, D.M., Benkovic, S.J. and Wright, P.E. (1995) *Biochemistry*, **34**, 11037–11048.

Fairbrother, W.J., Liu, J., Pisacane, P.I., Sliwkowski, M.X. and Palmer, A.G. (1998) *J. Mol. Biol.*, **279**, 1149–1161.

Farrow, N.A., Muhandiram, R., Singer, A.U., Pascal, S.M., Kay, C.M., Gish, G., Shoelson, S.E., Pawson, T., Forman-Kay, J.D. and Kay, L.E. (1994) *Biochemistry*, **33**, 5984–6003.

Farrow, N.A., Zhang, O., Szabo, A., Torchia, D.A. and Kay, L.E. (1995) *J. Biomol. NMR*, **6**, 153–162.

Frauenfelder, H. and McMahon, B. (1998) *Proc. Natl. Acad. Sci. USA*, **95**, 4795–4797.

Fushman, D. and Cowburn, D. (1998) *J. Am. Chem. Soc.*, **120**, 7109–7110.

Fushman, D. and Cowburn, D. (1999) *J. Biomol. NMR*, **13**, 139–147.

Fushman, D., Cahill, S. and Cowburn, D. (1997) *J. Mol. Biol.*, **266**, 173–194.

Fushman, D., Tjandra, N. and Cowburn, D. (1998) *J. Am. Chem. Soc.*, **120**, 10947–10952.

Fushman, D., Tjandra, N. and Cowburn, D. (1999) *J. Am. Chem. Soc.*, **121**, 8577–8582.

Gagné, S.M., Tsuda, S., Spyracopoulos, L., Kay, L.E. and Sykes, B.D. (1998) *J. Mol. Biol.*, **278**, 667–686.

Garcia de la Torre, J. and Bloomfield, V.A. (1981) *Quart. Rev. Biophys.*, **14**, 81–138.

Halle, B. and Wennerström, H. (1981) *J. Chem. Phys.*, **75**, 1928–1943.

Kay, L.E., Marion, D. and Bax, A. (1989a) *J. Magn. Reson.*, **84**, 72–84.

Kay, L.E., Torchia, D.A. and Bax, A. (1989b) *Biochemistry*, **28**, 8972–8979.

Korzhnev, D.M., Orekhov, V.Y. and Arseniev, A.S. (1997) *J. Magn. Reson.*, **127**, 184–191.

Kroenke, C.D., Loria, J.P., Lee, L.K., Rance, M. and Palmer, A.G. (1998) *J. Am. Chem. Soc.*, **120**, 7905–7915.

Lee, L.K., Rance, M., Chazin, W.J. and Palmer, A.G. (1997) *J. Biomol. NMR*, **9**, 287–298.

Lefèvre, J.-F., Dayie, K.T., Peng, J.W. and Wagner, G. (1996) *Biochemistry*, **35**, 2674–2686.

Lipari, G. and Szabo, A. (1982a) *J. Am. Chem. Soc.*, **104**, 4546–4559.

Lipari, G. and Szabo, A. (1982b) *J. Am. Chem. Soc.*, **104**, 4559–4570.

Luginbühl, P., Pervushin, K.V., Iwai, H. and Wüthrich, K. (1997) *Biochemistry*, **36**, 7305–7312.

Mandel, A.M., Akke, M. and Palmer, A.G. (1995) *J. Mol. Biol.*, **246**, 144–163.

Mandel, A.M., Akke, M. and Palmer, A.G. (1996) *Biochemistry*, **35**, 16009–16023.

Miller, G.P. and Bekovic, S.J. (1998) *Biochemistry*, **37**, 6327–6335.

Nicholson, L.K., Kay, L.E., Baldesseri, D.M., Arango, J., Young, P.E. and Torchia, D.A. (1992) *Biochemistry*, **31**, 5253–5263.

Orbons, L.P.M., van der Marel, G.A., van Boom, J.H. and Altona, C. (1987) *Eur. J. Biochem.*, **170**, 225–239.

Palmer, A.G., Rance, M. and Wright, P.E. (1991) *J. Am. Chem. Soc.*, **113**, 4371–4380.

Palmer, A.G., Williams, J. and McDermott, A. (1996) *J. Phys. Chem.*, **100**, 13293–13310.

Palmer, A.G. (2000) http://cpmcnet.columbia.edu/dept/gsas/biochem/labs/palmer/software.html

Pascual, J., Pfuhl, M., Rivas, G., Pastore, A. and Nilges, M. (1996) *FEBS Lett.*, **383**, 201–207.

Pascual, J., Pfuhl, M., Walther, D., Saraste, M. and Nilges, M. (1997) *J. Mol. Biol.*, **273**, 740–751.

Peng, J. and Wagner, G. (1992) *J. Magn. Reson.*, **98**, 308–332.

Peng, J. and Wagner, G. (1995) *Biochemistry*, **34**, 16733–16752.

Phan, I.Q.H., Boyd, J. and Campbell, I.D. (1996) *J. Biomol. NMR*, **8**, 369–378.

Sawaya, M.R. and Kraut, J. (1997) *Biochemistry*, **36**, 586–603.

Schurr, J.M., Babcock, H.P. and Fujimoto, B.S. (1994) *J. Magn. Reson.*, **B105**, 211–224.

Stivers, J.T., Abeygunawardana, C., Mildvan, A.S. and Whitman, C.P. (1996) *Biochemistry*, **35**, 16036–16047.

Stone, M.J., Fairbrother, W.J., Palmer, A.G., Reizer, J., Saier Jr., M.H. and Wright, P.E. (1992) *Biochemistry*, **31**, 4394–4406.
Stone, M.J., Chandrasekhar, K., Holmgren, A., Wright, P.E. and Dyson, H.J. (1993) *Biochemistry*, **32**, 426–435.
Tjandra, N., Feller, S.E., Pastor, R.W. and Bax, A. (1995b) *J. Am. Chem. Soc.*, **117**, 12562–12566.
Tjandra, N., Kuboniwa, H., Ren, H. and Bax, A. (1995a) *Eur. J. Biochem.*, **230**, 1014–1024.
Tjandra, N., Wingfield, P., Stahl, S. and Bax, A. (1996) *J. Biomol. NMR*, **8**, 273–284.
Tjandra, N., Garrett, D.S., Gronenborn, A.M., Bax, A. and Clore, G.M. (1997) *Nat. Struct. Biol.*, **4**, 443–449.
Van Tilborg, P.J.A., Mulder, F.A.A., de Backer, M.M.E., Nair, M., van Heerde, E.C., Folkers, G., van der Saag, P.T., Karimi Nejad, Y., Boelens, R. and Kaptein, R. (1999) *Biochemistry*, **38**, 1951–1956.
Woessner, D.E. (1962) *J. Chem. Phys.*, **37**, 647–654.
Yao, S., Hinds, M.G. and Norton, R.S. (1998) *J. Magn. Reson.*, **131**, 347–350.
Young, L. and Post, C.B. (1996) *Biochemistry*, **35**, 15129–15133.
Zheng, Z., Czaplicki, J. and Jardetzky, O. (1995) *Biochemistry*, **34**, 5212–5223.
Zhou, H.X., Wlodek, S.T. and McCammon, J.A. (1998) *Proc. Natl. Acad. Sci. USA*, **95**, 9280–9283.
Zinn-Justin, S., Berthault, P., Guenneugues, M. and Desvaux, H. (1997) *J. Biomol. NMR*, **10**, 363–372.